Institute of Parallel and Distributed Systems
University of Stuttgart
Universitätsstraße 38
D–70569 Stuttgart

Diplomarbeit Nr. 3203

Structural Properties of the Nested Period Incrementing Bifurcation Scenario

Ben W. Futter

Course of Study:	Engineering Cybernetics (Technische Kybernetik)
Examiner:	PD Dr. rer. nat. Michael Schanz
Supervisor:	PD Dr. rer. nat. habil. Viktor Avrutin

Commenced:	01. 03. 2011
Completed:	17. 08. 2011
CR-Classification:	G.2.0, J.2

Abstract

The importance of piecewise-smooth and especially that of discontinuous system models is well-established. One of the properties of these systems is the possibility of border collision bifurcations, which can form complex bifurcation scenarios. In this thesis, the description of the recently discovered nested period incrementing bifurcation scenario is significantly extended to form a more complete understanding of its topological structure. It is shown that the scenario is governed by codimension-two big bang bifurcations, in which well organised families of periodic orbits appear. The symbolic description of these families is determined by the unstable periodic orbits of the investigated system. This work introduces concise rules based on symbolic dynamics, by which the structure of the bifurcation scenario in the two-dimensional parameter space is fully described. It is furthermore shown that the results are easily transferred to discontinuous piecewise-linear systems defined on n partitions, in general.

Keywords: border collison bifurcation, big bang bifurcation, symbolic dynamics, U-sequence, discontinuous flat top tent map

Contents

List of Figures

List of Definitions and Theorems

1 Introduction

The main topic of this thesis is the bifurcation analysis of a particular class of time-discrete dynamical systems, which are given by one-dimensional maps defined on several partitions, featuring discontinuities and constant function branches. The importance of discontinuous and piecewise-smooth system models has been well established by now. Such systems are useful in many areas from engineering over biology to economics, and one of their key properties is the exhibition of so-called *border collision bifurcations* [5, 3, 6, 1].

Border collision bifurcations have been under steady investigation for over two decades, and there are several examples of bifurcation scenarios which are dominated by border collisions. One example is the well-known *period adding* scenario, which can be described using a Farey tree structure. Recently, the so-called *nested period incrementing* bifurcation scenario was discovered and investigated [2]. It constitutes a two-dimensional structure in parameter space and belongs to the class of border collision scenarios. The system for which the scenario can be observed, the so-called *discontinuous flat top tent map*, is defined on three partitions, on one of which the system function is constant. So far, all possible stable periodicity regions have been identified, as well as rules for their principal topology in one dimension of the bifurcation structure, which can be described by an infinite binary tree. This has given us a good understanding of the scenario on a "global" level. However, the mechanisms which generate the *families* of orbits which have been observed to emerge together within the scenario, have not yet been described.

In this work, the previous findings are significantly extended in order to better understand the nested period incrementing bifurcation scenario on a "local" level. This includes the investigation of codimension-two *big bang bifurcations*, which can be found all over the parameter space of the discontinuous flat top tent map. It turns out that these organising points, appearing in families along one dimension of the structure, generate local period incrementing cascades of new orbits within the already existing structure. The form of these new stable periodic orbits is thereby closely linked to the *unstable* orbits of the system.

The importance of these results is illustrated with the examination of a relevant system from economics. It is shown that this system can be investigated with the same techniques developed in this work, and that the results concerning the dynamical properties of the system are similar.

Outline

This thesis is structured as follows. In Sec. 2, the previous work on the nested period incrementing scenario is summarised, and terminology used for further investigation established.

Sec. 3 shows in detail, how the big bang bifurcations occurring in the investigated parameter space are organised, and in which way they generate new periodic orbits. The structure of all locally emerging families of cycles is discussed in Sec. 3.1. In Sec. 3.2 and 3.3, it is shown where the big bang bifurcations are located in parameter space, and how they are related to the well-known *period doubling scenario* and the closely related *U-sequence*. The role and types of codimension-one border collision bifurcations within this nested scenario are shortly presented in Sec. 3.4.

In Sec. 4, we see that some of the results for the discontinuous flat top tent map can also be transferred to similar systems with more than three partitions. First, an economic model is investigated and parallels to the previous results are presented. The investigative procedure used for this system is further generalised in Sec. 4.2 to the case of systems with arbitrarily many partitions.

The work is concluded with a short summary in Sec. 5.

2 The Discontinuous Flat Top Tent Map

The discontinuous flat top tent map is given by

$$x_{n+1} = f\big(x_n\big) \quad \text{with} \quad f(x) = \begin{cases} f_{\mathcal{L}}(x) = 2\alpha x & \text{if } x \leq \frac{1-\gamma}{2} \\ f_{\mathcal{C}}(x) = \beta & \text{if } \frac{1-\gamma}{2} < x < \frac{1+\gamma}{2} \\ f_{\mathcal{R}}(x) = 2\alpha(1-x) & \text{if } x \geq \frac{1+\gamma}{2}, \end{cases} \tag{2.1}$$

and this system's behavior of interest occurs in the parameter region (α, β) with

$$\alpha \in \left(\frac{1}{2}, \infty\right), \quad \beta \in [0,1] \quad \text{and} \quad \gamma = \text{const} \in (0,1).$$

The last parameter γ can be chosen constant, as it does not influence the qualitative bifurcation structure. (For numerical investigation, its value is assumed to be $\gamma = \frac{1}{10}$ unless explicitly noted otherwise.) Within these ranges the map's domain and image satisfy

$$f: \ [0,1] \to \big[0, \alpha(1-\gamma)\big] \cup \{\beta\},$$

so consequently, diverging orbits are possible if $\alpha > \alpha^\star = \frac{1}{1-\gamma}$.

2.1 Dynamical Properties

Fig. 2.1 shows four period and bifurcation diagrams, respectively, each of them for fixed α and varying β:

a) For $\alpha = 0.6$, we can see an interval where two symmetric incrementing cascades exist with an period increment of 1, accumulating at the boundaries of $\beta \in [0,1]$.

b) For $\alpha = 0.75$, the scenario as in a) is interrupted between any two adjacent periods, by a pair of incrementing cascades with a period increment of 2, accumulating at a common point.

c) For $\alpha = 0.85$, the scenario as in b) is interrupted between any two adjacent periods, by a pair of incrementing cascades with a period increment of 4.

d) At $\alpha = 0.9$, the scenario is already much further developed and the diagram already demonstrates the overall complexity of the fully developed bifurcation structure.

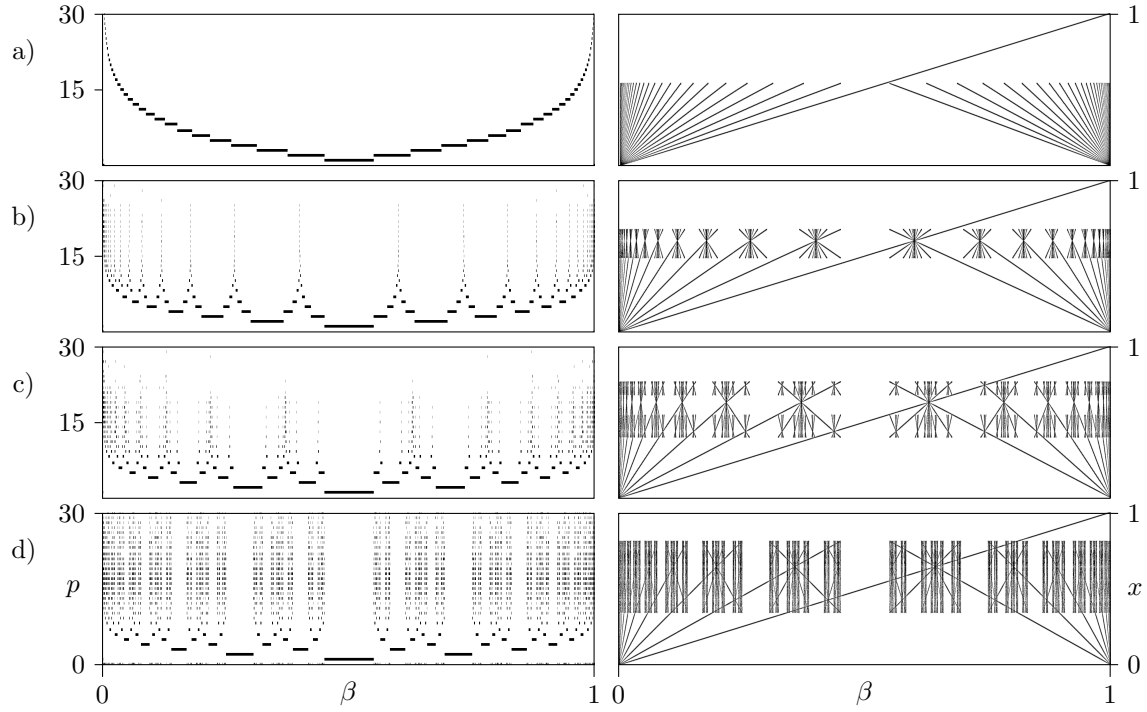

Figure 2.1: Representative period diagrams (left) and the corresponding bifurcation diagrams (right) for different values of α (compare Fig. 2.2) showing the following phenomena: a) pure period-1 incrementing scenario for $\alpha = 0.6$, b) pairs of opposed period-2 incrementing scenarios nested in-between for $\alpha = 0.75$, c,d) even further nesting for $\alpha = 0.85$ and $\alpha = 0.9$.

Due to the series of successively occurring nested period incrementing cascades, this scenario is referred to as *nested period incrementing*. Apparently, the complexity of the scenario increases with increasing α up to the value $\alpha^\star$. To explain this increasing complexity it is necessary to consider the bifurcation structure in the aforementioned 2D parameter region, which is presented in Fig. 2.2. This figure also indicates the locations of the 1D bifurcation diagrams presented in Fig. 2.1.

For increasing $\alpha \in \left[\frac{1}{2}, \alpha^\star\right]$, we see that new regions appear successively, giving rise to the mentioned increase in complexity. This process terminates at the value $\alpha = \alpha^\star$. Here, the situation is similar to that of the logistic map $x_{n+1} = ax_n(1-x_n)$ at $a = 4$. In both cases, the map becomes surjective, all possible periodic orbits (the stable three-partition orbits and the unstable two-partition orbits) exist—because all homoclinic bifurcations have already occurred—and the divergent behavior begins. Moreover, for $\alpha \to \infty$ we see that all non-diverging three-partition orbits accumulate at two organizing centers at $\beta = 0$ and $\beta = 1$.

In order to classify and distinguish all possible orbits, equation (2.1) is investigated with the familiar tools of symbolic dynamics, based on the system's natural partitions

$$I_{\mathcal{L}} = \left[0, \frac{1-\gamma}{2}\right], \quad I_{\mathcal{C}} = \left(\frac{1-\gamma}{2}, \frac{1+\gamma}{2}\right) \quad \text{and} \quad I_{\mathcal{R}} = \left[\frac{1+\gamma}{2}, 1\right].$$

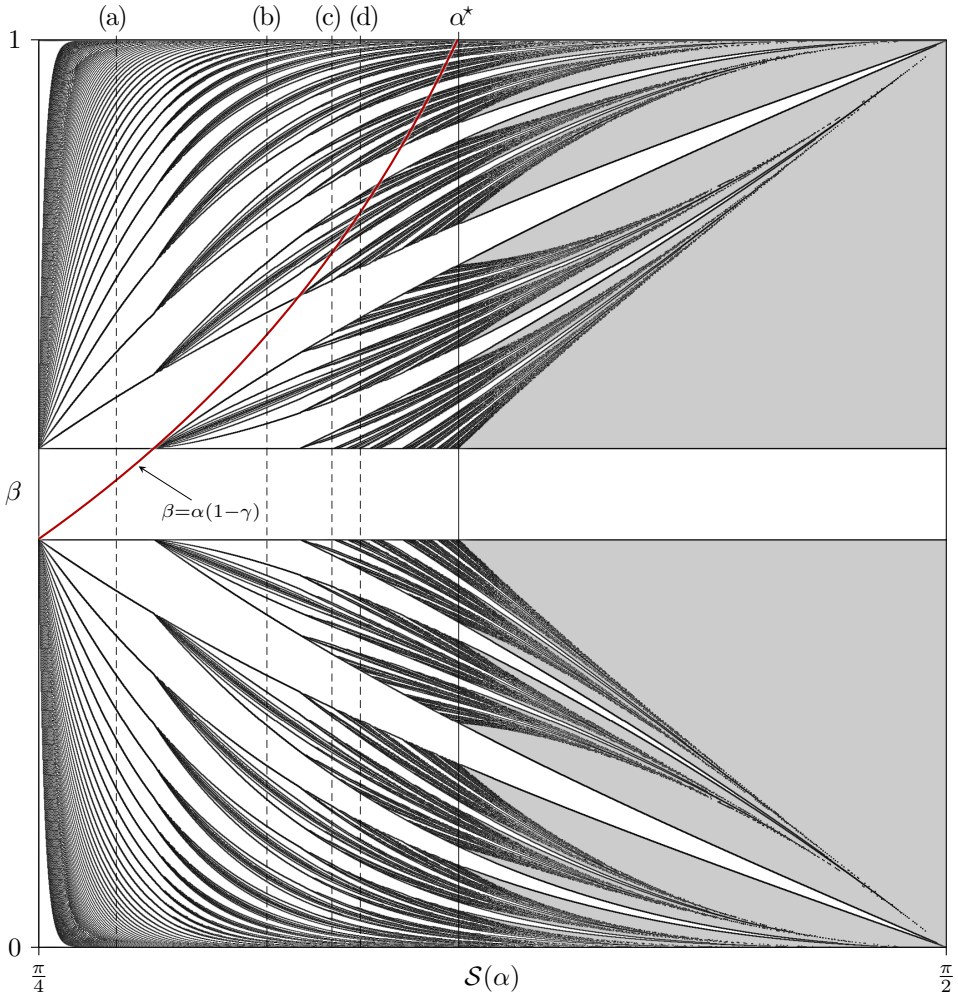

Figure 2.2: 2D bifurcation structure in the (α, β)-plane, for $\alpha \in \left(\frac{1}{2}, \infty\right)$, via the transformation $\mathcal{S}(\alpha) = \arctan(2\alpha)$. At $\alpha^\star$, diverging behavior (grey) becomes possible. The labels (a)–(d) indicate the locations of the 1D scenarios in Fig. 2.1.

For any orbit $\mathcal{O} = (x_0, x_1, x_2, \ldots, x_n)$ of the discontinuous flat top tent map, the corresponding symbolic sequence $s = s_0 s_1 s_2 \ldots s_n$ is defined, such that

$$s_i = \begin{cases} \mathcal{L} & \text{if } x_i \in I_\mathcal{L} \\ \mathcal{C} & \text{if } x_i \in I_\mathcal{C} \\ \mathcal{R} & \text{if } x_i \in I_\mathcal{R}. \end{cases}$$

This orbit can thereafter be unambiguously denoted as $\mathcal{O}_s$, and the periodicity region[1] of said orbit in parameter space as $\mathcal{P}_s$.

With this notation established, several important properties can be stated and easily checked, where the restrictions on the investigated parameter region formulated above

[1] or existence region

are assumed to hold:

Lemma 2.1 (Admissibility)**.** *Any admissible orbit $\mathcal{O}_s$ must satisfy*

$$\exists i\ (s_i = \mathcal{C}) \implies \nexists k\ (k \neq i \wedge s_k = \mathcal{C}),$$

i.e. the symbolic sequence s contains the symbol $\mathcal{C}$ no more than once. Therefore, any admissible symbolic sequence can be written as $s = \sigma$ or $s = \mathcal{C}\sigma$, where $\sigma \in \{\mathcal{L}, \mathcal{R}\}^n$.

Lemma 2.2 (Stability)**.** *The admissible limit cycle $\mathcal{O}_s$ is stable if and only if*

$$\exists i\ (s_i = \mathcal{C}),$$

i.e. the symbolic sequence s contains the symbol $\mathcal{C}$ exactly once.

Lemma 2.3 (Existence and Uniqueness)**.** *Assume $\alpha \geq \alpha^\star$. For all sequences σ, the unstable periodic orbits $\mathcal{O}_\sigma$ coexists independently of β. For every sequence $\mathcal{C}\sigma$, $\beta \in [0, 1]$ can be chosen such that the stable periodic orbit $\mathcal{O}_{\mathcal{C}\sigma}$ exists and is the unique stable orbit.*

Note: Lemma 2.3 does not hold for $\alpha < \alpha^\star$!

Lemma 2.4 (Stable Set)**.** *Assuming $\alpha \leq \alpha^\star$, the stable set[2] of any orbit intersecting $I_\mathcal{C}$ is dense in $[0, 1]$. Naturally, this includes all stable periodic orbits $\mathcal{O}_{\mathcal{C}\sigma}$.*
This implies that also the union of all periodicity regions $\bigcup \mathcal{P}_{\mathcal{C}\sigma}$ is dense in $[0, 1]$.

The existence of all stable orbits can be proved by induction using the following basic idea. Given a stable periodic orbit

$$f_\mathcal{C}\ \circlearrowright\ x_0 \xrightarrow{f_{\mathcal{L}/\mathcal{R}}} x_1 \xrightarrow{f_{\mathcal{L}/\mathcal{R}}} \cdots \xrightarrow{f_{\mathcal{L}/\mathcal{R}}} x_{n-1} \tag{2.2}$$

we can insert an extra iteration directly after the point $x_{n-1} \in I_\mathcal{C}$ by changing β to a preimage of the initial value x_0, which results in $f_\mathcal{C}(x) = f_{\mathcal{L}/\mathcal{R}}^{-1}(x_0)$:

$$f_\mathcal{C}\ \circlearrowright\ \overset{f_{\mathcal{L}/\mathcal{R}}^{-1}(x_0)}{=}\ x_n \xrightarrow{f_{\mathcal{L}/\mathcal{R}}} x_0 \xrightarrow{f_{\mathcal{L}/\mathcal{R}}} x_1 \xrightarrow{f_{\mathcal{L}/\mathcal{R}}} \cdots \xrightarrow{f_{\mathcal{L}/\mathcal{R}}} x_{n-1} \tag{2.3}$$

It is easy to check that the fixed point $\mathcal{O}_\mathcal{C}$ exists for $\beta \in I_\mathcal{C}$. All other stable orbits are obtained by recursive application of (2.2) and (2.3). This reasoning lets us obtain the periodicity region $\mathcal{P}_{\mathcal{C}\sigma}$ of any stable periodic orbit for fixed α as follows:

$$\mathcal{P}_{\mathcal{C}\sigma} = f_\sigma^{-1}\big(I_\mathcal{C}\big) = f_{\sigma_1}^{-1} \circ f_{\sigma_2}^{-1} \circ \cdots \circ f_{\sigma_{n-1}}^{-1}\big(I_\mathcal{C}\big) \tag{2.4}$$

This means that, given α, the n-periodic orbit $\mathcal{O}_{\mathcal{C}\sigma}$ exists if and only if $\beta \in \mathcal{P}_{\mathcal{C}\sigma}$ as determined by (2.4). For proofs of Lemmata 2.1–2.4 the reader is referred to [2].

[2] or basin of attraction

2.2 Complete Bifurcation Scenario

We can easily retrace the partitioning of the β-axis into periodicity regions with certain symbolic sequences. The locations of these regions are given by (2.4), as already stated. By applying this equation one symbol at a time, all regions can be calculated in a recursive manner: in the first step, it is only known that the interval $[0, 1]$ is subdivided (in β-ordering) into the three partitions $I_{\mathcal{L}}$, $\mathcal{P}_{\mathcal{C}}$ and $I_{\mathcal{R}}$. $\mathcal{P}_{\mathcal{C}} = I_{\mathcal{C}}$ is of course the existence region of the stable fixed point $\mathcal{O}_{\mathcal{C}}$, whereas the partitions $I_{\mathcal{L}}$ and $I_{\mathcal{R}}$ subsume all periodicity regions with the common prefix $\mathcal{CL}$ or $\mathcal{CR}$, respectively. For instance, any stable periodic orbit existing for $\beta \in I_{\mathcal{L}}$ has the point $x_1 \in I_{\mathcal{L}}$ and therefore must have a symbolic sequence beginning with $\mathcal{CL}$, possibly followed by further symbols.

Now, for $\alpha = \alpha^\star$ the function $f_{\mathcal{L}}^{-1}$ maps the interval $[0, 1]$ linearly onto the partition $I_{\mathcal{L}}$, which is therefore further subdivided into the following three partitions (one periodicity region and two common-prefix regions):

$$I_{\mathcal{L}^2} = f_{\mathcal{L}}^{-1}(I_{\mathcal{L}}), \quad \mathcal{P}_{\mathcal{CL}} = f_{\mathcal{L}}^{-1}\big(\mathcal{P}_{\mathcal{C}}\big), \quad I_{\mathcal{LR}} = f_{\mathcal{L}}^{-1}(I_{\mathcal{R}}) \tag{2.5}$$

For the right partition $I_{\mathcal{R}}$, the situation is the same, but as $f_{\mathcal{R}}^{-1}$ has a negative slope, the subdivision occurs in the opposite order:

$$I_{\mathcal{R}^2} = f_{\mathcal{R}}^{-1}(I_{\mathcal{R}}), \quad \mathcal{P}_{\mathcal{CR}} = f_{\mathcal{R}}^{-1}\big(\mathcal{P}_{\mathcal{C}}\big), \quad I_{\mathcal{RL}} = f_{\mathcal{R}}^{-1}(I_{\mathcal{L}}) \tag{2.6}$$

In summary, this procedure so far yields the following order of periodicity and common-prefix regions along $\beta \in [0, 1]$:

$$\underbrace{\underbrace{I_{\mathcal{L}^2} \quad \mathcal{P}_{\mathcal{CL}} \quad I_{\mathcal{LR}}}_{I_{\mathcal{L}}} \quad \mathcal{P}_{\mathcal{C}} \quad \underbrace{I_{\mathcal{R}^2} \quad \mathcal{P}_{\mathcal{CR}} \quad I_{\mathcal{RL}}}_{I_{\mathcal{R}}}}_{I=[0,1]} \tag{2.7}$$

Carried out ad infinitum, this procedure generates all sequences of stable orbits by subdividing the common-prefix regions level by level, the order of subdivision depending on the slope of the corresponding function branch, as explained for $f_{\mathcal{R}}^{-1}$ above. The sign of the slope of a function branch can be determined by the *parity* of the corresponding symbolic sequence, which is defined as follows:

Definition 2.1 (Parity; Even and Odd Sequences)**.**
The parity of a symbolic sequence $s = s_1 s_2 \dots s_n$ is defined as

$$\operatorname{par} s = \left(\sum_{i=1}^{n} \operatorname{par}\big(s_i\big) \right) \bmod 2,$$
$$\textit{where } \operatorname{par}\big(\mathcal{L}\big) = 0, \ \operatorname{par}\big(\mathcal{C}\big) = 0 \textit{ and } \operatorname{par}\big(\mathcal{R}\big) = 1.$$

Sequences with $\operatorname{par} s = 0$ *are called* even*, whereas sequences with* $\operatorname{par} s = 1$ *are* odd*.*

It is easy to check that the function branch $f_\sigma = f_{\sigma_n} \circ \cdots \circ f_{\sigma_2} \circ f_{\sigma_1}$ has a slope, the sign of which is given by $(-1)^{\mathrm{par}\,\sigma}$. From the preceding argument, the following basic property of the discontinuous flat top tent map can be deduced:

Theorem 2.1 (β-Order)**.** *For fixed α, the total order of periodicity regions along the parameter $\beta \in [0,1]$ is equivalent to the complete binary tree generated by the rules*

- *The root node contains the sequence $\mathcal{C}$.*
- *To each node with the* even *sequence $\mathcal{C}\sigma$*
  - *add a child node containing $\mathcal{C}\sigma\mathcal{L}$ to the left*
  - *add a child node containing $\mathcal{C}\sigma\mathcal{R}$ to the right.*
- *To each node with the* odd *sequence $\mathcal{C}\sigma$*
  - *add a child node containing $\mathcal{C}\sigma\mathcal{R}$ to the left*
  - *add a child node containing $\mathcal{C}\sigma\mathcal{L}$ to the right.*

This binary tree is denoted as the suffix tree*. The resulting order is increasing in β from left to right.*

It follows from Lemma 2.3 and Theorem 2.1 that, for $\alpha = \alpha^\star$, the structure of the stable periodic orbits for $\beta \in [0,1]$ is completely determined by the suffix tree. For this reason, we refer to the case at $\alpha^\star$ as the *complete bifurcation scenario.*

For $\alpha > \alpha^\star$ the situation is qualitatively the same, except for the additional possibility of diverging dynamics. By contrast, for $\alpha < \alpha^\star$ much less periodic orbits exist, and hence not every sequence is possible. To understand the reason for this, consider equation (2.4) for obtaining the periodicity region of $\mathcal{O}_{\mathcal{C}\sigma}$. It must be guaranteed that each preimage along the "inversion chain" in (2.4) lies (at least partially) within the proper domain, i.e.

$$\begin{aligned} f_{\sigma_{n-1}}^{-1}\big(I_{\mathcal{C}}\big) \cap I_{\sigma_{n-1}} &\neq \emptyset \\ f_{\sigma_{n-2}}^{-1} \circ f_{\sigma_{n-1}}^{-1}\big(I_{\mathcal{C}}\big) \cap I_{\sigma_{n-2}} &\neq \emptyset \\ &\vdots \\ f_\sigma^{-1}\big(I_{\mathcal{C}}\big) = f_{\sigma_1}^{-1} \circ f_{\sigma_2}^{-1} \circ \cdots \circ f_{\sigma_{n-1}}^{-1}\big(I_{\mathcal{C}}\big) \cap\ I_{\sigma_1} &\neq \emptyset \end{aligned}$$

For $\alpha = \alpha^\star$ all points in $[0,1]$ have two preimages under $f_{\mathcal{L}/\mathcal{R}}$, and so these conditions are satisfied for all possible sequences $\mathcal{C}\sigma$. With $\alpha < \alpha^\star$ this is no longer the case. For practical reasons it may be noted that the preimages of an arbitrary interval (a,b) evaluate to:

$$\begin{aligned} f_{\mathcal{L}}^{-1}\Big((a,b)\Big) &= \big(\tfrac{a}{2\alpha}, \tfrac{b}{2\alpha}\big) \cap I_{\mathcal{L}}, \\ f_{\mathcal{R}}^{-1}\Big((a,b)\Big) &= \big(1-\tfrac{b}{2\alpha}, 1-\tfrac{a}{2\alpha}\big) \cap I_{\mathcal{R}} \end{aligned}$$

With this restriction, (2.4) may lead to $\mathcal{P}_{\mathcal{C}\sigma} = \emptyset$ for certain sequences and particular choices of α. In this case the orbit $\mathcal{O}_{\mathcal{C}\sigma}$ does not exist in these parameter regions.

2.3 Milnor Attractors

So far, the only attractors which have been considered are the stable orbits of the discontinuous flat top tent map, i.e. the limit cycles containing a point in $I_{\mathcal{C}}$. These occur when the parameter β is chosen such that $f_{\mathcal{C}}$ maps the middle interval into one of its preimages. There are however singular situations when an altogether different behaviour emerges, namely when β is not located in one of the periodicity regions, but on one of the numerous *unstable* orbits, or preimages thereof.

For instance, consider the most simple case $\beta = 0$. From the initial value $x_0 = \frac{1}{2}$, the orbit is mapped to the unstable fixed point $x_1 = 0$ in one iteration, where it remains in absence of disturbance. If the orbit is driven away ever so slightly from the unstable fixed point, it will eventually reach the interval $I_{\mathcal{C}}$ and then the unstable fixed point again, according to Lemma 2.4. The same is the case for $\beta = f_{\mathcal{R}}^{-1}(0) = 1$, although here the orbit, after reaching $I_{\mathcal{C}}$, first makes an additional iteration in $I_{\mathcal{R}}$ before reaching the fixed point. Attractors of this kind are commonly denoted as Milnor attractors or weak attractors.

The regions in parameter space, where an unstable orbit $\mathcal{O}_\sigma$ becomes a Milnor attractor shall be denoted by $\mathcal{B}_\sigma$. This is of course the set of pre-periodic points of $\mathcal{O}_\sigma = (x_1, x_2, \ldots, x_n)$, which are given by the preimages $f_\varrho^{-1}(x_1)$ of the unstable orbit's innermost point[3]. Each of these particular points is given by $\mathcal{B}_\sigma^\varrho$, so that $\mathcal{B}_\sigma = \bigcup \mathcal{B}_\sigma^\varrho$. This notation is still ambiguous, as $f_\varrho^{-1}(x_1) = f_{\varrho\sigma^n}^{-1}(x_1)$. Therefore, ϱ shall always be chosen as the *shortest, non-empty sequence* out of all sequences which would lead to the same point. For varying α, $\mathcal{B}_\sigma$ becomes a set of curves in parameter space. Furthermore, the number of curves in $\mathcal{B}_\sigma$ increases whenever the unstable orbit $\mathcal{O}_\sigma$ undergoes a homoclinic bifurcation. In that case, more preimages of $\mathcal{O}_\sigma$ become available and so a whole family of new "paths" ϱ to the Milnor attractor are possible.

Although Milnor attractors only exist on a set of Lebesgue measure zero in parameter space, and are therefore structurally unstable, we will see that these attractors as well as their location play an important role as accumulation points of the minor incrementing cascades that lead to the complete scenario. Under certain conditions, the existence of the pre-periodic point $\mathcal{B}_\sigma^\varrho$ implies the existence of a family of stable orbits with the symbolic sequences $\mathcal{C}\varrho\sigma^n$.

[3] see also Definition 3.1 on page 12

3 Nested Structures

By now we have a description of the fully developed bifurcation scenario for $\alpha \geq \alpha^\star$, where all possible unstable orbits $\mathcal{O}_{\{\mathcal{L},\mathcal{R}\}^n}$ and stable orbits $\mathcal{O}_{\mathcal{C}\{\mathcal{L},\mathcal{R}\}^n}$ exist. For $\frac{1}{2} < \alpha < \alpha^\star$ we know how the periodicity regions $\mathcal{P}_{\mathcal{C}\sigma}$ are ordered over the parameter β. We have also seen that the discontinuous flat top tent map displays a simple incrementing structure for small α, as well as some levels of embedded incrementing structures with higher period-increments. But of all the concrete bifurcation scenarios occurring along the way, little is known so far.

It turns out that the successive emergence of unstable orbits provides a skeleton for the stable periodicity regions, which becomes increasingly complex and eventually evolves into the structure already described.

3.1 Accumulation Curves and Big Bang Bifurcations

In Fig. 3.1 we see the curve in parameter space where $I_\mathcal{C}$ is mapped directly onto the unstable fixed point in the right partition, and where this fixed point consequently becomes a Milnor attractor. For those values of α, where this curve does not yet exist, the bifurcation scenario consists of the periodicity region of the stable fixed point $\mathcal{O}_\mathcal{C}$, plus two incrementing cascades for increasing and decreasing β on either side. Explicitly marked are the periodicity regions (up to period 6) of the orbits forming these two cascades, namely orbits of the form $\mathcal{C}(\mathcal{L}|\mathcal{R})\mathcal{L}^n$.[1]

This situation changes at $\alpha = \alpha_\mathcal{R}$. Here we see a codimension-2 bifurcation where a region emerges between $\mathcal{P}_\mathcal{C}$ and $\mathcal{P}_{\mathcal{C}\mathcal{R}}$, at the heart of which lies the Milnor attractor curve $\mathcal{B}^\mathcal{R}_\mathcal{R}$. Within this region, there is an incrementing cascade of periodicity regions $\mathcal{P}_{\mathcal{C}\mathcal{R}\mathcal{R}^n}$, $n \geq 1$, approaching $\mathcal{B}^\mathcal{R}_\mathcal{R}$ in an alternating fashion, i.e. with even n to one side of the accumulation point, and odd n to the other.

From the symmetry of the discontinuous flat top tent map we know that, on the other side of the interval $I_\mathcal{C}$, the same scenario occurs between $\mathcal{P}_\mathcal{C}$ and $\mathcal{P}_{\mathcal{C}\mathcal{L}}$, with the incrementing cascade $\mathcal{P}_{\mathcal{C}\mathcal{L}\mathcal{R}^n}$, $n \geq 1$ and accumulation curve $\mathcal{B}^\mathcal{L}_\mathcal{R}$. In fact, we can see similar bifurcations occurring all over the parameter plane. As we know that all periodicity regions are related to the fixed point periodicity region as backward orbits thereof (2.4), it is clear that all scenarios occurring in the vicinity of $\mathcal{P}_\mathcal{C}$ can be transferred to all other existing regions $\mathcal{P}_{\mathcal{C}\sigma}$. Organizing centers like these, which create

[1] This family of sequences could also be written as $\mathcal{C}\mathcal{R}^{\{0,1\}}\mathcal{L}^n$, but the notation that was chosen better reflects the general symmetry of the bifurcation scenario: for each orbit $\mathcal{O}_{\mathcal{C}\mathcal{L}\sigma}$ existing for some $\beta = \beta'$, there is an orbit $\mathcal{O}_{\mathcal{C}\mathcal{R}\sigma}$ at $\beta = 1 - \beta'$ and vice versa.

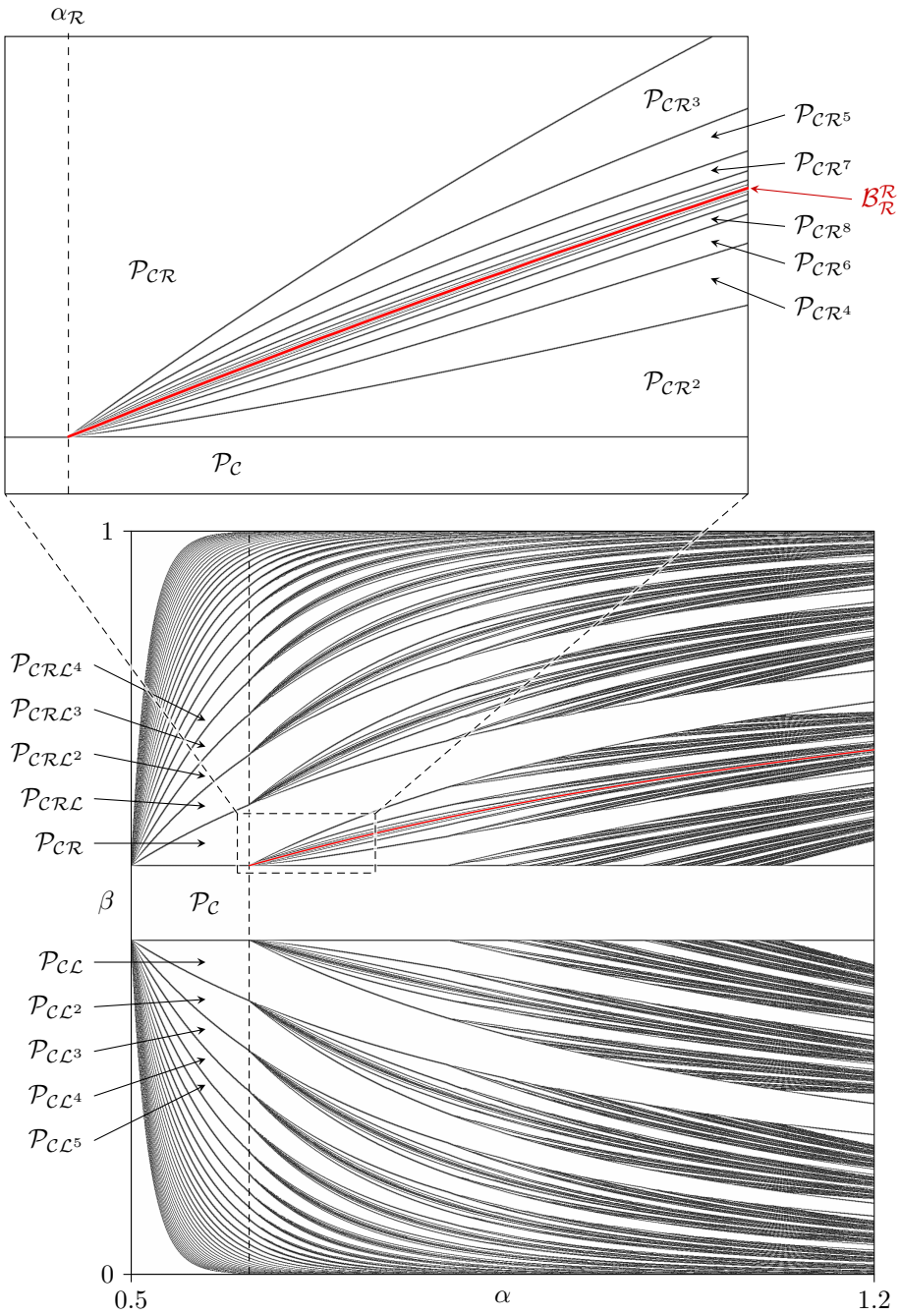

Figure 3.1: Blowup of a big bang bifurcation associated with the unstable fixed point $\mathcal{O}_{\mathcal{R}}$. At this point, the curve $\mathcal{B}^{\mathcal{R}}_{\mathcal{R}}$ emerges where $\mathcal{O}_{\mathcal{R}}$ becomes a Milnor attractor, along with a family of periodicity regions $\mathcal{P}_{\mathcal{CR}^n}$ associated with this attractor.

an infinitude of periodicity regions, are commonly known as *big bang bifurcations*. It stands to reason that these systematically give rise to the families of stable orbits which eventually form the complete scenario described in Sec. 2.2.

These big bang bifurcations and the resulting incrementing cascades appear at those points in state space and parameter space, where the associated Milnor attractors come into existence. Because the unstable orbits of the discontinuous flat top tent map structurally coincide with those of the well-known tent map, but are virtual as long as some of their points lie in the middle partition, we must regard the region where the last of these points passes a border of $I_\mathcal{C}$.

Definition 3.1 (Canonical Sequence)**.** *The representation $\mathcal{O}_\sigma = (x_1, x_2, \ldots, x_n)$ of an unstable orbit and its sequence $\sigma = \sigma_1\sigma_2\ldots\sigma_n \in \{\mathcal{L}, \mathcal{R}\}^n$ shall be denoted* canonical *if*

$$\forall\, i = 2\ldots n \quad \left| x_1 - \frac{1}{2} \right| < \left| x_i - \frac{1}{2} \right|,$$

i.e. the (symbolic) representation starts with the orbit's innermost point x_1, which is denoted for all orbits by x_1^σ.

Definition 3.2 (Emerging Point)**.** *For each unstable orbit $\mathcal{O}_\sigma$ the* emerging point *α_σ is the value of the parameter α for which the orbit's innermost point lies on the boundary of $I_\mathcal{C}$, i.e.*

$$x_1^\sigma \in \left\{ \frac{1-\gamma}{2}, \frac{1+\gamma}{2} \right\}.$$

As stated above, the unstable orbit $\mathcal{O}_\sigma$ is virtual for $\alpha < \alpha_\sigma$, whereas for $\alpha > \alpha_\sigma$ the orbit exists with one point very near the flat interval $I_\mathcal{C}$. There are now two possible cases.

3.1.1 Incrementing Cascade for Odd Orbits

First, we consider an unstable orbit with the canonical sequence σ and *odd* parity at $\alpha = \alpha_\sigma + \varepsilon$ slightly beyond its emerging point, where $\varepsilon > 0$ is chosen such that

$$f_\sigma^2\big(x_\mathrm{b}\big) \in I_\mathcal{C} \quad \text{where} \quad x_\mathrm{b} = \begin{cases} \frac{1+\gamma}{2} & \text{if } \sigma_1 = \mathcal{R} \\ \frac{1-\gamma}{2} & \text{if } \sigma_1 = \mathcal{L} \end{cases} \tag{3.1}$$

This situation is depicted in a neighbourhood of $I_\mathcal{C}$ in Fig. 3.2. The red dashed path shows that (3.1) holds, in which case we say that α is in the *emerging domain* of the odd unstable orbit $\mathcal{O}_\sigma$.

Now regard the periodicity regions $\mathcal{P}_{\mathcal{C}\sigma^n}$, assuming, without loss of generality, that σ starts with the symbol $\mathcal{R}$:

- For the orbit $\mathcal{O}_{\mathcal{C}\sigma}$ we have $\mathcal{P}_{\mathcal{C}\sigma} = f_\sigma^{-1}\big(I_\mathcal{C}\big) = \Big(f_\sigma^{-1}(\frac{1+\gamma}{2}), f_\sigma^{-1}(\frac{1-\gamma}{2})\Big)$. Note that this orbit already exists for $\alpha < \alpha_\sigma$ with $\mathcal{P}_{\mathcal{C}\sigma} = f_\sigma^{-1}\big(I_\mathcal{C}\big) = \Big[\frac{1+\gamma}{2}, f_\sigma^{-1}(\frac{1-\gamma}{2})\Big)$.

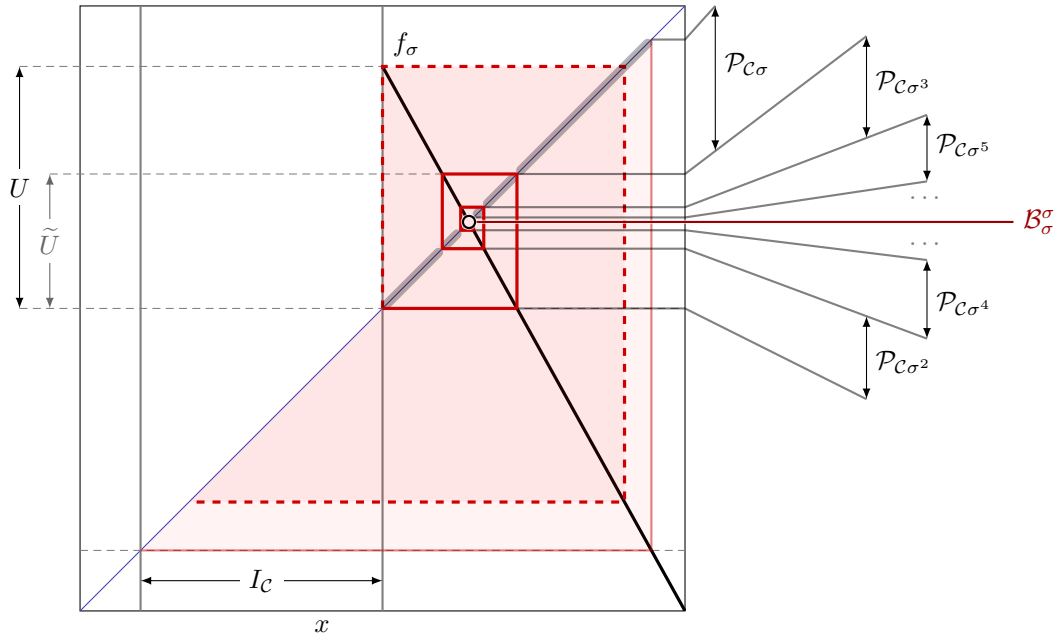

Figure 3.2: Schematic of an incrementing cascade for $\alpha = \alpha_\sigma + \varepsilon$ in a neighbourhood of the middle partition, where $\sigma = \mathcal{R}\sigma_2\sigma_3\ldots\sigma_n$ is the canonical sequence of an *odd* orbit.

- For the orbit $\mathcal{O}_{\mathcal{C}\sigma^2}$ we get $\mathcal{P}_{\mathcal{C}\sigma^2} = f_\sigma^{-2}(I_\mathcal{C}) = \left[\frac{1+\gamma}{2}, f_\sigma^{-2}(\frac{1+\gamma}{2})\right)$, which is directly adjacent to $\mathcal{P}_\mathcal{C}$.
- For the orbit $\mathcal{O}_{\mathcal{C}\sigma^3}$ we get $\mathcal{P}_{\mathcal{C}\sigma^3} = f_\sigma^{-3}(I_\mathcal{C}) = \left(f_\sigma^{-3}(\frac{1+\gamma}{2}), f_\sigma^{-1}(\frac{1+\gamma}{2})\right]$, which is directly adjacent to $\mathcal{P}_{\mathcal{C}\sigma}$.
- Consequently, all regions $\mathcal{P}_{\mathcal{C}\sigma^n}$, $n > 2$, lie densely between $\mathcal{P}_{\mathcal{C}\sigma^2}$ and $\mathcal{P}_{\mathcal{C}\sigma}$, and approach the (for f_σ^{-1} stable) focus $\mathcal{O}_\sigma$ from alternating sides.

In summary there is a neighbourhood (cf. Fig. 3.2)

$$\widetilde{U} = \left[\tfrac{1+\gamma}{2}, f_\sigma^{-1}\left(\tfrac{1+\gamma}{2}\right)\right], \quad \text{satisfying} \quad \widetilde{U} = \left(\bigcup_{i=1}^{\infty} \mathcal{P}_{\mathcal{C}\sigma\sigma^i}\right) \cup \mathcal{B}^\sigma_\sigma, \tag{3.2}$$

which subsumes all orbits of the new incrementing cascade. We can think of this cascade as "belonging to" the (already existing) orbit $\mathcal{O}_{\mathcal{C}\sigma}$. From the viewpoint of the fixed point $\mathcal{O}_\mathcal{C}$, basically the same scenario is given by the region

$$U = f_\sigma\left(\widetilde{U}\right) = \left[\tfrac{1+\gamma}{2}, f_\sigma^{-1}\left(\tfrac{1+\gamma}{2}\right)\right],$$

which additionally includes part of $\mathcal{P}_{\mathcal{C}\sigma}$. Due to the system's symmetry, the same scenario takes place on the other side of $I_\mathcal{C}$, yet mirrored and all sequences beginning

with $\mathcal{L}$. In conclusion the local scenario around $I_{\mathcal{C}}$ in the emerging domain of $\mathcal{O}_\sigma$ is given by:

$$\mathcal{P}_{\mathcal{C}\bar{\sigma}} \overbrace{\left| \mathcal{P}_{\mathcal{C}\bar{\sigma}\sigma^2} \right| \mathcal{P}_{\mathcal{C}\bar{\sigma}\sigma^4} \cdots \mathcal{B}_{\bar{\sigma}} \cdots \mathcal{P}_{\mathcal{C}\bar{\sigma}\sigma^3} \left| \mathcal{P}_{\mathcal{C}\bar{\sigma}\sigma} \right.}^{\text{cascade associated with } \mathcal{P}_{\mathcal{C}\bar{\sigma}} \ (\beta \in 1-\widetilde{U})} \left| \mathcal{P}_{\mathcal{C}} \right| \underbrace{\overbrace{\left| \mathcal{P}_{\mathcal{C}\sigma\sigma} \right| \mathcal{P}_{\mathcal{C}\sigma\sigma^3} \cdots \mathcal{B}_{\sigma} \cdots \mathcal{P}_{\mathcal{C}\sigma\sigma^4} \left| \mathcal{P}_{\mathcal{C}\sigma\sigma^2} \right.}^{\text{cascade associated with } \mathcal{P}_{\mathcal{C}\sigma} \ (\beta \in \widetilde{U})} \left| \mathcal{P}_{\mathcal{C}\sigma} \right.}_{\text{cascade associated with } \mathcal{P}_{\mathcal{C}} \ (\beta \in U)},$$

where we define the *mirrored orbit* of σ as

$$\bar{\sigma} = S\sigma_2\sigma_3 \ldots \sigma_n, \quad S = \begin{cases} \mathcal{L} & \text{if } \sigma_1 = \mathcal{R} \\ \mathcal{R} & \text{if } \sigma_1 = \mathcal{L}, \end{cases}$$

i.e. the orbit obtained by inverting the first symbol.

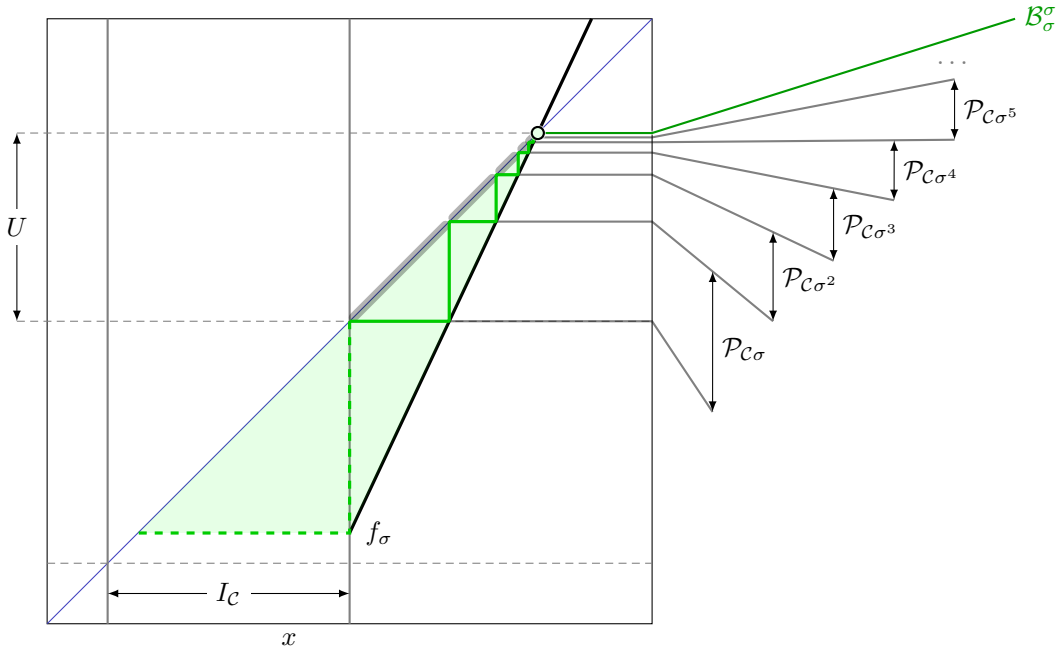

Figure 3.3: Schematic of an incrementing cascade for $\alpha = \alpha_\sigma + \varepsilon$ in a neighbourhood of the middle partition, where $\sigma = \mathcal{R}\sigma_2\sigma_3 \ldots \sigma_n$ is the canonical sequence of an *even* orbit.

3.1.2 Incrementing Cascade for Even Orbits

In the case that the considered unstable orbit with the canonical sequence σ is *even*, the situation is slightly different, as shown in Fig. 3.3. Again, we observe the point x_1^σ of $\mathcal{O}_\sigma$ at $\alpha = \alpha_\sigma + \varepsilon$. Now however, $\varepsilon > 0$ is chosen such that

$$f_\sigma(x_{\mathrm{b}}) \in I_{\mathcal{C}} \quad \text{where} \quad x_{\mathrm{b}} = \begin{cases} \frac{1+\gamma}{2} & \text{if } \sigma_1 = \mathcal{R} \\ \frac{1-\gamma}{2} & \text{if } \sigma_1 = \mathcal{L} \end{cases} \tag{3.3}$$

(Note the difference in the iteration order compared to (3.1).) This situation is depicted in a neighbourhood of $I_{\mathcal{C}}$ in Fig. 3.3. Here, when (3.3) holds, we say that α is in the emerging domain of the *even* unstable orbit $\mathcal{O}_\sigma$.

Again assuming that σ starts with the symbol $\mathcal{R}$, we regard the periodicity regions $\mathcal{P}_{\mathcal{C}\sigma^n}$:

- For the orbit $\mathcal{O}_{\mathcal{C}\sigma}$ we have $\mathcal{P}_{\mathcal{C}\sigma} = f_\sigma^{-1}\big(I_{\mathcal{C}}\big) = \Big[\frac{1+\gamma}{2}, f_\sigma^{-1}(\frac{1+\gamma}{2})\Big)$, which is already directly adjacent to $\mathcal{P}_{\mathcal{C}}$.
- Consequently, all regions $\mathcal{P}_{\mathcal{C}\sigma^n}$, $n > 1$, lie densely side by side and approach the (for f_σ^{-1} stable) node $\mathcal{O}_\sigma$ from below.

Now the containing neighbourhood U (cf. Fig. 3.3) is given by

$$U = \Big[\tfrac{1+\gamma}{2}, x_1^\sigma\Big], \quad \text{satisfying} \quad U = \left(\bigcup_{i=0}^{\infty} \mathcal{P}_{\mathcal{C}\sigma\sigma^i}\right) \cup \mathcal{B}_\sigma^\sigma. \tag{3.4}$$

Due to the system's symmetry, the same scenario takes place on the other side of $I_{\mathcal{C}}$, yet mirrored and all sequences beginning with $\mathcal{L}$. This mirror-scenario is contained to the region

$$1 - U = \Big[1 - x_1^\sigma, \tfrac{1-\gamma}{2}\Big], \quad \text{satisfying} \quad 1 - U = \left(\bigcup_{i=0}^{\infty} \mathcal{P}_{\mathcal{C}\bar\sigma\sigma^i}\right) \cup \mathcal{B}_\sigma^{\bar\sigma}. \tag{3.5}$$

In conclusion the local scenario around $I_{\mathcal{C}}$ in the emerging domain of $\mathcal{O}_\sigma$ is given by:

$$\underbrace{\mathcal{B}_\sigma^{\bar\sigma} \cdots \mathcal{P}_{\mathcal{C}\bar\sigma\sigma^4} \,\big|\, \mathcal{P}_{\mathcal{C}\bar\sigma\sigma^3} \,\big|\, \mathcal{P}_{\mathcal{C}\bar\sigma\sigma^2} \,\big|\, \mathcal{P}_{\mathcal{C}\bar\sigma\sigma} \,\big|\, \mathcal{P}_{\mathcal{C}\bar\sigma}}_{\text{left cascade associated with } \mathcal{P}_{\mathcal{C}} \ (\beta \in 1-U)} \,\big|\, \mathcal{P}_{\mathcal{C}} \,\big|\, \underbrace{\mathcal{P}_{\mathcal{C}\sigma} \,\big|\, \mathcal{P}_{\mathcal{C}\sigma\sigma} \,\big|\, \mathcal{P}_{\mathcal{C}\sigma\sigma^2} \,\big|\, \mathcal{P}_{\mathcal{C}\sigma\sigma^3} \,\big|\, \mathcal{P}_{\mathcal{C}\sigma\sigma^4} \cdots \mathcal{B}_\sigma^\sigma}_{\text{right cascade associated with } \mathcal{P}_{\mathcal{C}} \ (\beta \in U)}$$

3.1.3 Conclusion

For both cases that have been examined above, the scenario can be transferred to all periodicity regions already existing at the emerging point α_σ. Let the set of all periodicity regions $\mathcal{P}_{\mathcal{C}\varrho}$ existing for $\alpha < \alpha_\sigma$ be given by $\mathbb{P}_\sigma$. As shown in Sec. 2.1, these regions are given as preimages of $I_{\mathcal{C}}$ in parameter space. Therefore, the scenario observed at a boundary of the fixed point region $\mathcal{P}_{\mathcal{C}}$ can also be observed at the boundaries of other periodicity regions $\mathcal{P}_{\mathcal{C}\varrho}$. Depending on the parity of ϱ, the derived scenario occurs either in the same direction (ϱ even), or mirrored (ϱ odd). Also, for any sequence $\mathcal{C}s$ in the original cascade, each derived orbit is given by $\mathcal{C}\varrho s$. From the preceding observations, the following two central theorems are easily derived.

Theorem 3.1 (Odd Incrementing Cascade)**.** *Consider the emerging point α_σ of an unstable orbit $\mathcal{O}_\sigma$ with* odd *parity. Now assume $\alpha > \alpha_\sigma$ in the emerging domain given by* (3.1)*. In the neighbourhood of each periodicity region $\mathcal{P}_{\mathcal{C}\varrho} \in \mathbb{P}_\sigma$ there is an*

alternating *cascade of new periodicity regions* $\mathcal{P}_{\mathcal{C}\varrho\sigma^k}$, $k \geq 1$, *approaching the point* $\mathcal{B}^{\varrho}_{\varrho}$. *The position of this cascade relative to* $\mathcal{P}_{\mathcal{C}\varrho}$ *thereby depends on the parity of* ϱ *and the first symbol of* σ *in the following way:*

$$\begin{aligned} &\mathcal{P}_{\mathcal{C}\varrho} \overset{k}{\longrightarrow} \mathcal{P}_{\mathcal{C}\varrho\sigma^{2k}} \cdots \mathcal{B}^{\varrho}_{\sigma} \cdots \overset{k}{\longleftarrow} \mathcal{P}_{\mathcal{C}\varrho\sigma^{2k-1}} && \text{if } \operatorname{par}(\sigma_1\varrho) = 1, \\ &\underset{k}{\longrightarrow} \mathcal{P}_{\mathcal{C}\varrho\sigma^{2k-1}} \cdots \mathcal{B}^{\varrho}_{\sigma} \cdots \underset{k}{\longleftarrow} \mathcal{P}_{\mathcal{C}\varrho\sigma^{2k}} \mathcal{P}_{\mathcal{C}\varrho} && \text{if } \operatorname{par}(\sigma_1\varrho) = 0. \end{aligned}$$

Theorem 3.2 (Even Incrementing Cascade)**.** *Consider the emerging point* α_σ *of an unstable orbit* $\mathcal{O}_\sigma$ *with* even *parity. Now assume* $\alpha > \alpha_\sigma$ *in the emerging domain given by* (3.3)*. In the neighbourhood of each periodicity region* $\mathcal{P}_{\mathcal{C}\varrho} \in \mathbb{P}_\sigma$ *there are* two monotonic *cascades of new periodicity regions* $\mathcal{P}_{\mathcal{C}\varrho\sigma^{k+1}}$, $\mathcal{P}_{\mathcal{C}\varrho\bar{\sigma}\sigma^k}$, $k \geq 0$, *approaching the points* $\mathcal{B}^{\varrho}_{\varrho}$ *and* $\mathcal{B}^{\bar{\varrho}}_{\varrho}$*. The position of these cascades relative to* $\mathcal{P}_{\mathcal{C}\varrho}$ *thereby depends on the parity of* ϱ *and the first symbol of* σ *in the following way:*

$$\begin{aligned} &\mathcal{B}^{\varrho\bar{\sigma}}_{\sigma} \cdots \overset{k}{\longleftarrow} \mathcal{P}_{\mathcal{C}\varrho\bar{\sigma}\sigma^k} \mathcal{P}_{\mathcal{C}\varrho} \overset{k}{\longrightarrow} \mathcal{P}_{\mathcal{C}\varrho\sigma^{k+1}} \cdots \mathcal{B}^{\varrho\sigma}_{\sigma} && \text{if } \operatorname{par}(\sigma_1\varrho) = 1, \\ &\mathcal{B}^{\varrho\sigma}_{\sigma} \cdots \underset{k}{\longleftarrow} \mathcal{P}_{\mathcal{C}\varrho\sigma^{k+1}} \mathcal{P}_{\mathcal{C}\varrho} \underset{k}{\longrightarrow} \mathcal{P}_{\mathcal{C}\varrho\bar{\sigma}\sigma^k} \cdots \mathcal{B}^{\varrho\bar{\sigma}}_{\sigma} && \text{if } \operatorname{par}(\sigma_1\varrho) = 0. \end{aligned}$$

Knowing the local structures of these big bang bifurcations and how they are determined by the Milnor attractors which emerge at these points, it would be interesting to know in which of these unstable orbits appear at which stage. That means, how are the emerging points α_σ ordered for increasing α? As the unstable orbits are independent of β, we can answer this question by regarding a special case of the discontinuous flat top tent map, namely the case where the map is continuous. This case has already been under thorough investigation by several authors, and the appearance of unstable orbits is readily explained.

3.2 Digression: Period-Doubling Cascades

The continuous case of (2.1) satisfies $\beta = \alpha(1-\gamma)$, and yields the well-known *flat top tent map* given by

$$f(x) = \begin{cases} f_{\mathcal{L}}(x) = 2\alpha x & \text{if } x \leq \frac{1-\gamma}{2} \\ f_{\mathcal{C}}(x) = \alpha(1-\gamma) & \text{if } \frac{1-\gamma}{2} < x < \frac{1+\gamma}{2} \\ f_{\mathcal{R}}(x) = 2\alpha(1-x) & \text{if } x \geq \frac{1+\gamma}{2}. \end{cases} \tag{3.6}$$

This location of this case in parameter space is graphically represented in Fig. 2.2 as a red curve.[2] The system belongs to the class of unimodal maps under consideration in

[2] Although linear for fixed γ, the relationship $\beta = \alpha(1-\gamma)$ becomes a curve in this figure, as the bifurcation diagram is scaled in α in order to accommodate values approaching infinity.

the famous work [4] by Metropolis-Stein-Stein, who developed a recursive set of rules for determining the α-order of the flat top tent map's stable periodic orbits.

Their main result was that the prototypical bifurcation scenario in unimodal maps—being governed by flip and fold bifurcations—is made up from period doubling cascades. Using a symbolic notation equivalent to the one used in this thesis, the authors showed that the successive orbits in such a cascade are determined by their so-called *harmonic* and *anti-harmonic extensions*. These results will be briefly reiterated, starting with the following definition.

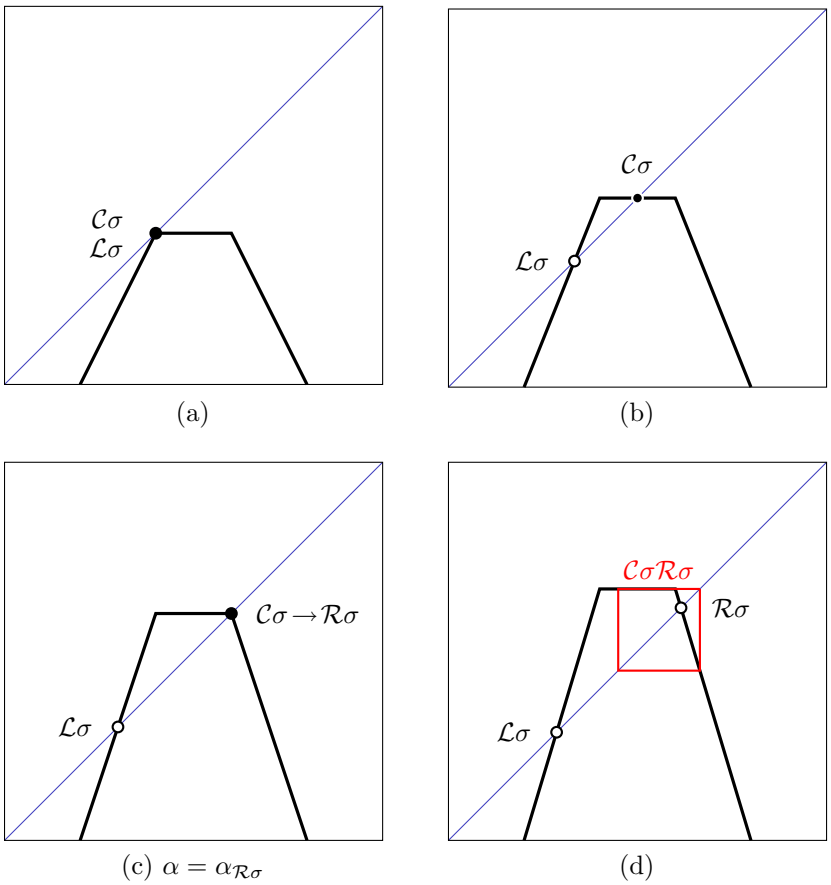

Figure 3.4: The higher order iterate f^n in a neighbourhood of $I_{\mathcal{C}}$ for increasing α: (a) saddle-node bifurcation creating the orbits $\mathcal{C}\sigma$ (stable) and $\mathcal{L}\sigma$ (unstable), (b) situation within the $\mathcal{C}\sigma$-window, (c) the stable cycle $\mathcal{C}\sigma$ crosses the right border and becomes $\mathcal{R}\sigma$ (unstable), whereby the stable orbit $\mathcal{C}\sigma\mathcal{R}\sigma$ emerges (d). In this case, σ is a word of length $n-1$ with even parity. *Remark:* Note that these schematics are not to scale! In particular, the branches $f_{\mathcal{L}\sigma}$ and $f_{\mathcal{R}\sigma}$ may vanish in figure (a).

Definition 3.3 (Harmonic and Anti-Harmonic Symbol)**.** *The* harmonic *and* anti-harmonic symbol *of a symbolic sequence* σ *are defined as*

$$\mathcal{H}(\sigma) = \begin{cases} \mathcal{R} & \text{if } \sigma \text{ is even} \\ \mathcal{L} & \text{if } \sigma \text{ is odd,} \end{cases} \qquad \mathcal{A}(\sigma) = \begin{cases} \mathcal{L} & \text{if } \sigma \text{ is even} \\ \mathcal{R} & \text{if } \sigma \text{ is odd,} \end{cases}$$

respectively.

The transition from one stable orbit $\mathcal{O}_{\mathcal{C}\sigma}$ to its period-doubled successor is depicted from the view of the iterate f^n in Figs. 3.4 and 3.5, for even and odd sequences σ, respectively. We see there that, first, the stable orbit with the symbolic sequence $\mathcal{C}\sigma$ emerges along with the unstable orbit $\mathcal{A}(\sigma)\sigma$. Subsequently, the stable orbit crosses the border and two orbits emerge: the unstable $\mathcal{H}(\sigma)\sigma$ and the stable period-doubled orbit $\mathcal{C}\sigma\mathcal{H}(\sigma)\sigma = \mathcal{C}\widetilde{\sigma}$. The location of this latter bifurcation in parameter space is of course what we earlier defined as the emerging point $\alpha_{\mathcal{H}(\sigma)\sigma}$.

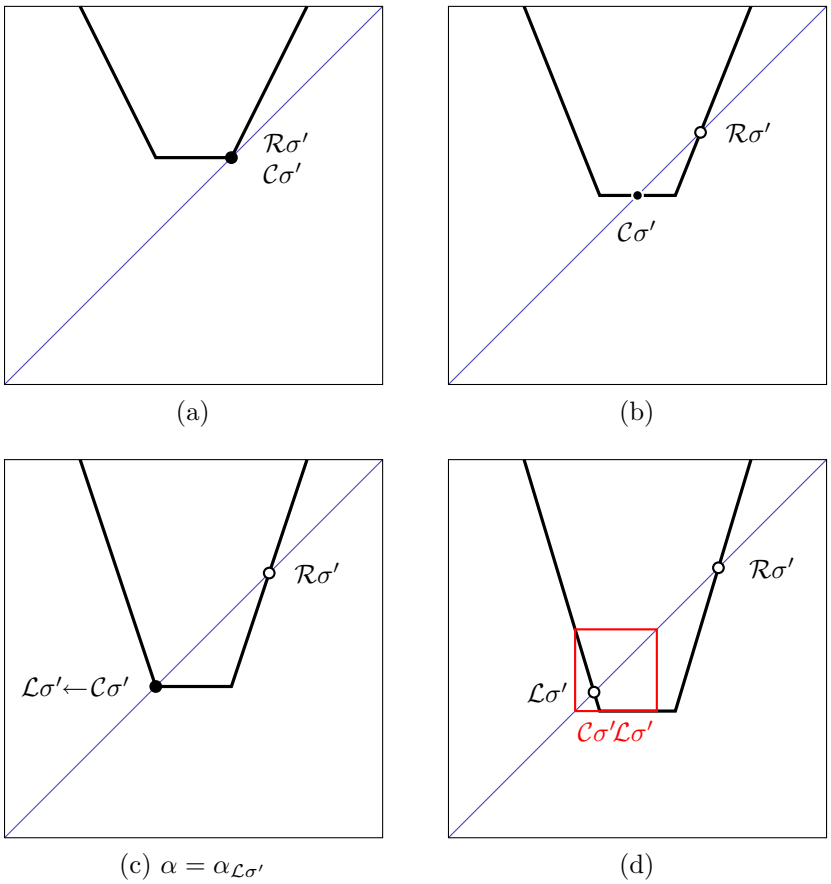

Figure 3.5: The converse case of Fig. 3.4, where σ' is a word with *odd* parity. If $\sigma' = \sigma\mathcal{R}\sigma$, then (a) depicts the higher order iterate f^{2n} at the same point $\alpha = \alpha_{\mathcal{R}\sigma}$ as Fig. 3.4c. In that case, this figure represents the next step in the same period doubling cascade.

Here the process repeats itself with the appearance of $\mathcal{C}\widetilde{\sigma}$ and $\mathcal{A}(\widetilde{\sigma})\widetilde{\sigma}$, which is of course simply $\mathcal{A}\big(\sigma\mathcal{H}(\sigma)\sigma\big)\sigma\mathcal{H}(\sigma)\sigma = \big(\mathcal{H}(\sigma)\sigma\big)^2$, and so forth.

Lemma 3.1 (Doubling Operator for Stable Orbits)**.** *The operator generating the symbolic sequence of the next stable orbit in a period doubling cascade, based on that of the preceding orbit $\mathcal{O}_{\mathcal{C}\sigma}$, is given by*

$$\mathrm{D}_{\mathcal{H}} : \ \mathcal{C}\sigma \mapsto \mathcal{C}\sigma\mathcal{H}(\sigma)\sigma$$

and shall be denoted as the harmonic doubling operator*. For convenience, the* anti-harmonic *doubling operator is defined accordingly:*

$$\mathrm{D}_{\mathcal{A}} : \ \mathcal{C}\sigma \mapsto \mathcal{C}\sigma\mathcal{A}(\sigma)\sigma.$$

This explains all stable orbits occurring in a period-doubling cascade, beginning with a certain orbit $\mathcal{O}_{\mathcal{C}\sigma}$. This "base sequence" can also be determined from the rules given by Metropolis-Stein-Stein, here slightly paraphrased:

Lemma 3.2 (Base Seqences of the Period-Doubling Cascades)**.** *The first base sequence in α-order is given by $\mathcal{C}$, the last is given by $\mathcal{CRL}^{\infty}$. Between any two adjacent base sequences s_1 and s_2 (given in α-order) there is a third base sequence s, which is given by the longest common prefix of the (infinite) sequences $\mathrm{D}_{\mathcal{H}}^{\infty}(s_1)$ and $\mathrm{D}_{\mathcal{A}}^{\infty}(s_2)$. The complete α-order of base sequences follows from recursion.*

To get a raw image of the resulting structure, here are the α-ordered base sequences after three iterations of this rule:

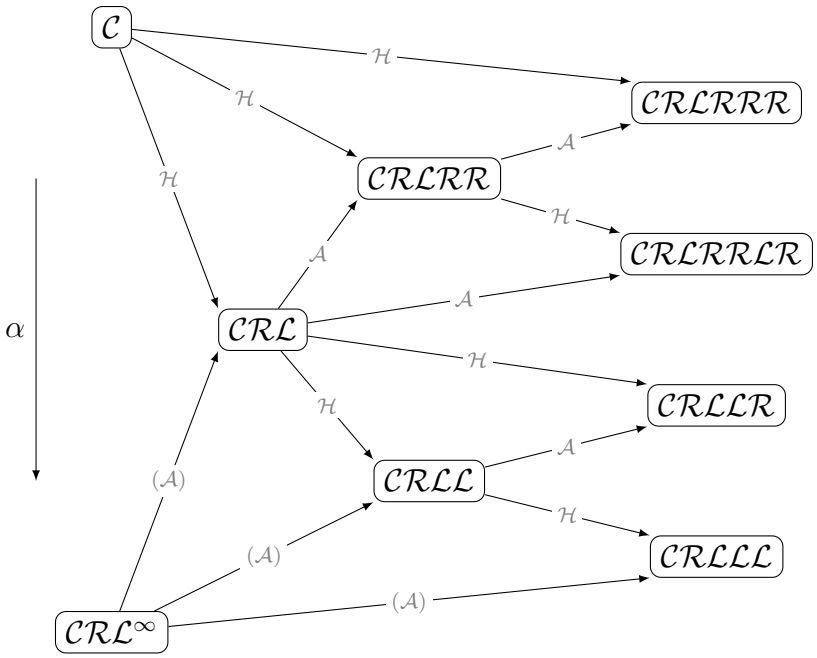

3.2.1 Map Replacement

While the recursive application of $\mathrm{D}_{\mathcal{H}}$ is sufficient to generate the complete doubling cascade following an arbitrary base sequence, it is also worth noting that all these cascades can be derived directly from the first doubling cascade via map replacement.

Lemma 3.3 (Map Replacement)**.** *Assume a given base sequence $\mathcal{C}\varrho$ represents a feasible orbit of the flat top tent map. Then the sequences of the doubling cascade $\{\mathcal{C}\varrho, \mathcal{C}\varrho\mathcal{H}(\varrho)\varrho \ldots\}$ associated with this sequence can be obtained from the prototypical cascade $\{\mathcal{C}, \mathcal{CR}, \mathcal{CRLCR} \ldots\}$ by applying the following symbolic replacement:*

$$\mathrm{MR}_{\varrho}(\sigma) : \begin{cases} \mathcal{L} & \mapsto & \mathcal{A}(\varrho)\varrho \\ \mathcal{C} & \mapsto & \mathcal{C}\varrho \\ \mathcal{R} & \mapsto & \mathcal{H}(\varrho)\varrho. \end{cases}$$

Note: This rule satisfies $\operatorname{len}\big(\mathrm{MR}_{\varrho}(\sigma)\big) = \operatorname{len}(\sigma)\cdot\operatorname{len}\big(\mathcal{C}\varrho\big)$, and also $\operatorname{par}\mathrm{MR}_{\varrho}(\sigma) = \operatorname{par}\sigma$, which follows from Definition 3.3, i.e. this replacement rule preserves parity.

Proof. Consider a sequence $\mathcal{C}\sigma$ from the first doubling cascade.

a) Doubling the sequence and then applying the replacement rules gives

$$\mathcal{C}\sigma \xrightarrow{\mathrm{D}_{\mathcal{H}}} \mathcal{C}\sigma\mathcal{H}(\sigma)\sigma \xrightarrow{\mathrm{MR}_{\varrho}} \mathcal{C}\varrho\,\mathrm{MR}_{\varrho}(\sigma)\,\mathrm{MR}_{\varrho}\big(\mathcal{H}(\sigma)\big)\,\mathrm{MR}_{\varrho}(\sigma).$$

b) Applying map replacement first and then doubling results in

$$\mathcal{C}\sigma \xrightarrow{\mathrm{MR}_{\varrho}} \mathcal{C}\varrho\,\mathrm{MR}_{\varrho}(\sigma) \xrightarrow{\mathrm{D}_{\mathcal{H}}} \mathcal{C}\varrho\,\mathrm{MR}_{\varrho}(\sigma)\,\mathcal{H}\big(\varrho\,\mathrm{MR}_{\varrho}(\sigma)\big)\varrho\,\mathrm{MR}_{\varrho}(\sigma).$$

It is easy to check that $\mathrm{MR}_{\varrho}\big(\mathcal{H}(\sigma)\big) = \mathcal{H}(\varrho\sigma)\varrho = \mathcal{H}\big(\varrho\,\mathrm{MR}_{\varrho}(\sigma)\big)\varrho$, simply by performing a case-by-case analysis of the different parity constellations. Therefore, $\mathrm{D}_{\mathcal{H}}$ and MR_{ϱ} are commutative. The rest follows from induction, noting that $\mathrm{MR}_{\varrho}(\mathcal{C}) = \mathcal{C}\varrho$. □

Note that the replacement rule MR_{ϱ} is of course also valid if used to obtain the *unstable* orbits in a period doubling cascade with a given base sequence from the canonical sequences of the unstable orbits in the first cascade. In this case, the sequences which the replacement rules yield are also in canonical form, as $\mathcal{L}\varrho$ and $\mathcal{R}\varrho$ (the first two orbits to appear in a cascade) must be canonical sequences if $\mathcal{O}_{\mathcal{C}\varrho}$ is an admissible orbit of the flat top tent map.

3.3 Big Bang Bifurcation Cascades

So much for the stable periodic orbits of the flat top tent map. As stated earlier, the emergence of the accompanying *unstable* orbits in the explanation of the doubling cascade does not depend on the map's middle partition, and is therefore equally valid

for the discontinuous flat top tent map and the occurrence of the incrementing cascades explained in Sec. 3.1.1 and 3.1.2. Note that—as a result of the structure of the doubling cascades—*even* unstable orbits only emerge at the very beginning of a period-doubling cascade. Therefore, the beginning of such a cascade is marked by the emerging point α_σ of an even unstable orbit, and all further steps by the emerging points of the subsequent odd orbits.

Theorem 3.3 (Doubling Operator for Unstable Orbits)**.** *The operator generating the symbolic sequence of the next emerging point in a period doubling cascade, based on that of the preceding sequence σ, is given by*

$$\mathrm{D}_u : \sigma \mapsto \begin{cases} \bar{\sigma} = \mathcal{H}(\sigma_1)\sigma_2 \ldots \sigma_n & \text{if } \operatorname{par}\sigma = 0 \\ \bar{\sigma}\sigma = \mathcal{H}(\sigma_1)\sigma_2 \ldots \sigma_n\sigma_1\sigma_2 \ldots \sigma_n & \text{if } \operatorname{par}\sigma = 1. \end{cases}$$

Proof. If σ is even, then the corresponding emerging point α_σ marks the beginning of a period-doubling cascade, and the next unstable orbit in the cascade is given by $\bar{\sigma}$, as shown in Sec. 3.2. The statement for odd orbits follows easily from Lemma 3.1, since

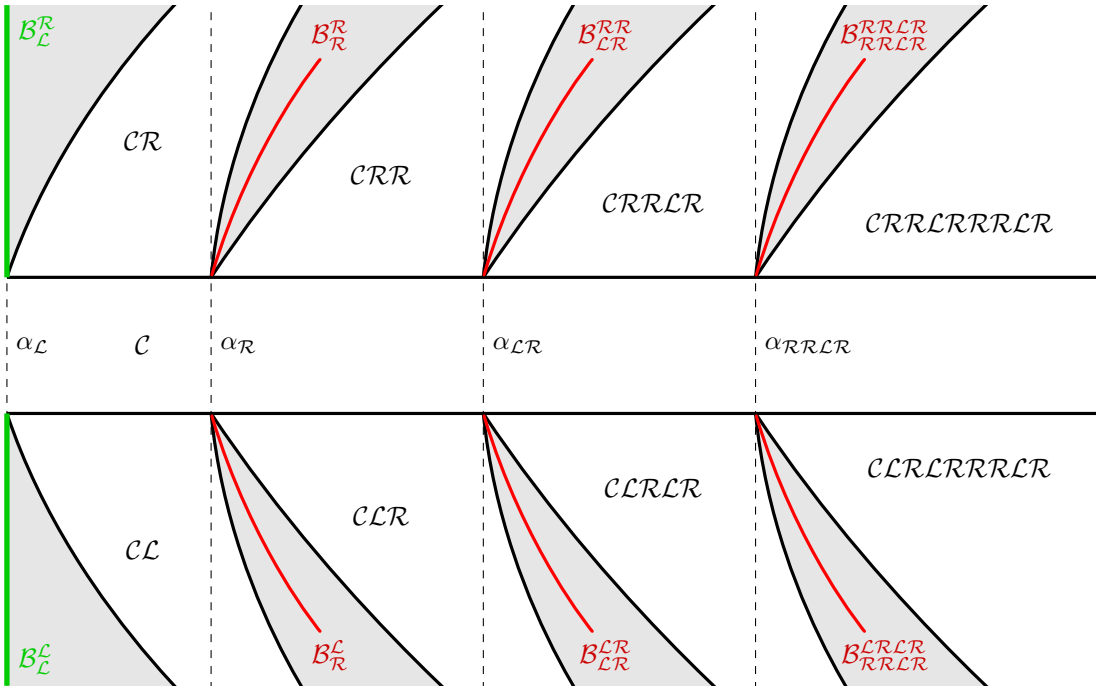

Figure 3.6: Schematic of the Big Bang Cascade starting at the emerging point $\alpha_{\mathcal{L}}$ in the neighbourhood of $I_{\mathcal{C}}$. Each grey region around the Milnor curve $\mathcal{B}^{\varrho}_{\sigma}$ contains a cascade with the sequences $\mathcal{C}\varrho\sigma^n$.

doubling the sequence $\mathcal{C}\sigma$ twice yields

$$\mathrm{D}_{\mathcal{H}}\big(\mathcal{C}\sigma\big) = \mathcal{C}\sigma\underbrace{\mathcal{H}(\sigma)\sigma}_{\sigma^{I}} \quad \text{and} \quad \begin{aligned}\mathrm{D}^2_{\mathcal{H}}\big(\mathcal{C}\sigma\big) &= \mathcal{C}\sigma\mathcal{H}(\sigma)\sigma\mathcal{H}\Big(\sigma\mathcal{H}(\sigma)\sigma\Big)\sigma\mathcal{H}(\sigma)\sigma \\ &= \mathcal{C}\sigma\mathcal{H}(\sigma)\sigma\underbrace{\mathcal{H}^2(\sigma)\sigma\mathcal{H}(\sigma)\sigma}_{\sigma^{II}},\end{aligned}$$

and clearly $\sigma^{II} = \mathrm{D}_u\big(\sigma^{I}\big)$. □

As stated in Theorems 3.1 and 3.2, at each emerging point α_σ occurs an infinitude of big bang bifurcations, with a family of stable periodic orbits created from each one. The α-order of these emerging points can be determined by the aforementioned rules.

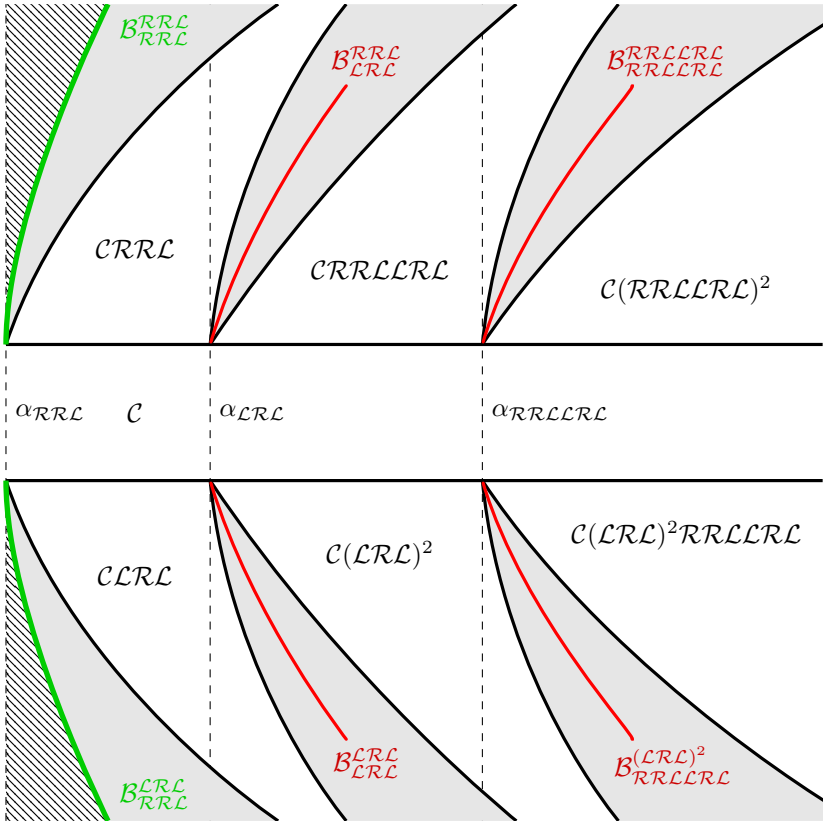

Figure 3.7: Schematic of the Big Bang Cascade starting at the emerging point $\alpha_{\mathcal{RRL}}$ in the neighbourhood of $I_{\mathcal{C}}$. Each grey region around the Milnor curve $\mathcal{B}^{\varrho}_{\sigma}$ contains a cascade with the sequences $\mathcal{C}\varrho\sigma^n$. The hatched area contains orbits already existing at $\alpha_{\mathcal{RRL}}$, i.e. orbits with sequences $s \in L_{\mathcal{RRL}}$.

Theorem 3.4 (Complete Big Bang Bifurcation Scenario)**.** *For each base sequence $\mathcal{C}\varrho$ given by Lemma 3.2, there is a series of emerging points α_σ^k, $k = 0 \ldots \infty$, with $\sigma^k = \mathrm{D}_u^k\big(\mathcal{A}(\varrho)\varrho\big)$. The only stable periodic orbit existing for $\alpha < \alpha_\mathcal{L}$ is the fixed point $\mathcal{O}_\mathcal{C}$. The set of stable periodic orbits generated by each subsequent emerging point is given by Theorems 3.1 and 3.2.*

This theorem gives a complete and concise description of the two-dimensional nested period incrementing bifurcation scenario, as occurring in the (α, β) parameter plane of the discontinuous flat top tent map, including all big bang bifurcations contained therein and the families of symbolic sequences these big bangs generate. Practically, this statement should be taken with a grain of salt. Already at the end of the first doubling cascade, i.e. for $\alpha > \alpha_{\mathrm{D}_u^\infty(\mathcal{L})}$, it is obviously not possible to enumerate all existing periodic orbits in a closed form. After all, the very structure of successive nesting in Lemma 3.2 does not permit us to determine the following adjacent base sequence in α-order.

However, if a maximal period for all stable orbits under consideration is fixed a priori, the number of emerging points α_σ becomes finite, and the procedure of enumerating all stable orbits pretty much straightforward.

To get an impression of the complexity of the bifurcation structure, which the discontinuous flat top tent map produces, we can take a brief look at two concrete cascades of big bang bifurcations. The very first of these cascades occurs at the emerging point $\alpha_\mathcal{L} = \frac{1}{2}$, and a schematic of the big bang bifurcations of this cascade occurring in the vicinity of $I_\mathcal{C}$ is shown in Fig. 3.6. The emerging points of this scenario are given by

$$\alpha_\mathcal{L} < \alpha_\mathcal{R} < \alpha_{\mathcal{LR}} < \alpha_{\mathcal{RRLR}} < \alpha_{\mathcal{LRLRRRLR}} < \cdots$$

As already known, the set of stable periodic orbits existing for $\alpha < \alpha_\mathcal{L}$ contains only the fixed point $\mathcal{O}_\mathcal{C}$. The set of all symbolic sequences existing for $\alpha < \alpha_\sigma$ shall be denoted as L_σ and so we have $L_\mathcal{L} = \big\{\mathcal{C}\big\}$. The orbits emerging at $\alpha_\mathcal{L}$ follow from Theorem 3.2, and so the sequences existing before the next emerging point $\alpha_\mathcal{R}$ are given by

$$L_{\mathrm{D}_u(\mathcal{L})} = L_\mathcal{R} = \big\{\mathcal{C}, \mathcal{CL}, \mathcal{CL}^2, \ldots, \mathcal{CR}, \mathcal{CRL}, \mathcal{CRL}^2, \ldots\big\} = L_\mathcal{L} \cup \big\{\mathcal{C}(\mathcal{L}|\mathcal{R})\mathcal{L}^k \mid k \geq 0\big\}.$$

The orbits emerging next follow from Theorem 3.1, and so all sequences existing for $\alpha_\mathcal{R} < \alpha < \alpha_{\mathcal{LR}}$ are given by

$$L_{\mathrm{D}_u(\mathcal{R})} = L_{\mathcal{LR}} = L_\mathcal{R} \cup \big\{\mathcal{C}\varrho\mathcal{R}^k \mid \mathcal{C}\varrho \in L_\mathcal{R}, k \geq 1\big\}.$$

These sequences of course form the basis for all orbits which exist just after the next emerging point $\alpha_{\mathcal{LR}}$:

$$L_{\mathrm{D}_u(\mathcal{LR})} = L_{\mathcal{RRLR}} = L_{\mathcal{LR}} \cup \big\{\mathcal{C}\varrho(\mathcal{LR})^k \mid \mathcal{C}\varrho \in L_{\mathcal{LR}}, k \geq 1\big\}.$$

Generally, for this first doubling cascade, the set of symbolic sequences existing before any emerging point $\alpha_{\mathrm{D}_u(\sigma)}$ is given by $L_{\mathrm{D}_u(\sigma)} = L_\sigma \cup \big\{\mathcal{C}\varrho\sigma^k \mid \mathcal{C}\varrho \in L_\sigma, k \geq 1\big\}$, and

consequently, the set of symbolic sequences generated in the big bang bifurcations of the preceding emerging point α_σ can be given completely as $G_\sigma = L_{\mathrm{D}_u(\sigma)} \setminus L_\sigma$. At any point along this first doubling cascade, the set of all orbits created so far can be described in a closed form

$$L_{\mathrm{D}_u^{i+1}(\mathcal{L})} = \left\{\mathcal{C}\mathcal{R}^{\{0,1\}}\mathcal{L}^a(\mathcal{L}\mathcal{R})^b(\mathcal{R}\mathcal{R}\mathcal{L}\mathcal{R})^c \ldots (\mathrm{D}_u^i(\mathcal{L}))^k \mid a, b, c, \ldots, k \geq 0\right\},$$

as can the set $G_{\mathrm{D}_u^i(\mathcal{L})}$ of all orbits *created* at any emerging point $\alpha_{\mathrm{D}_u^i(\mathcal{L})}$. But for significantly larger values of α the same can, of course, no longer be said.

Fig. 3.7 shows the doubling cascade which starts at the emerging point $\alpha_{\mathcal{R}\mathcal{R}\mathcal{L}}$ and is therefore located somewhat further along the α-axis. The families of orbits which can be found in this cascade are obtained in the same manner:

$$\begin{aligned} L_{\mathcal{L}\mathcal{R}\mathcal{L}} &= L_{\mathcal{R}\mathcal{R}\mathcal{L}} \cup \left\{\mathcal{C}\varrho(\mathcal{R}\mathcal{R}\mathcal{L})^k \mid \mathcal{C}\varrho \in L_{\mathcal{R}\mathcal{R}\mathcal{L}}, k \geq 1\right\} \quad \text{for} \quad \alpha_{\mathcal{R}\mathcal{R}\mathcal{L}} < \alpha < \alpha_{\mathcal{L}\mathcal{R}\mathcal{L}} \\ L_{\mathcal{R}^2\mathcal{L}^2\mathcal{R}\mathcal{L}} &= L_{\mathcal{L}\mathcal{R}\mathcal{L}} \cup \left\{\mathcal{C}\varrho(\mathcal{L}\mathcal{R}\mathcal{L})^k \mid \mathcal{C}\varrho \in L_{\mathcal{L}\mathcal{R}\mathcal{L}}, k \geq 1\right\} \quad \text{for} \quad \alpha_{\mathcal{L}\mathcal{R}\mathcal{L}} < \alpha < \alpha_{\mathcal{R}^2\mathcal{L}^2\mathcal{R}\mathcal{L}} \\ &\vdots \end{aligned}$$

Note, however, that we have no closed expression for the set of symbolic sequences $L_{\mathcal{R}\mathcal{R}\mathcal{L}}$ which exist for $\alpha < \alpha_{\mathcal{R}\mathcal{R}\mathcal{L}}$. As a consequence, it is not possible to list all orbits appearing at $\alpha_{\mathcal{R}\mathcal{R}\mathcal{L}}$, but we do know that all these orbits share a characteristic $(\mathcal{R}\mathcal{R}\mathcal{L})^k$ suffix.

3.4 Border Collision Curves

Much has been said so far about the codimension-2 big bang bifurcations, in which—prosaically put—all periodic orbits "are born". Also of interest are the codimension-1 bifurcations in the nested period incrementing scenario, which separate one periodicity region from the other. These are of the *border collision* (BC) type, which is a typical situation for piecewise-smooth and discontinuous systems.

The BC bifurcations in this scenario are fairly "harmless", as they always lead from one globally stable periodic orbit to another, or to diverging behaviour. In other systems, especially those exhibiting chaos, the transition of dynamical behaviour at a border collision can be of a much more radical nature. For more information on border collision bifurcations, the reader is referred to [5, 3, 6].

The simplest case of border collision can be observed for the case of the fixed point $\mathcal{O}_\mathcal{C}$ which is given by $x = \beta$. This orbit exists only for $\beta \in \mathcal{P}_\mathcal{C} = I_\mathcal{C}$, as we have already seen. If β crosses either the left $\left(\frac{1-\gamma}{2}\right)$ or right border $\left(\frac{1+\gamma}{2}\right)$ of the partition $I_\mathcal{C}$, the fixed point ceases to exist. These two BC bifurcations are given by

$$\Psi_\mathcal{C}^l = \left\{(\alpha, \beta) \;\middle|\; \beta = \frac{1-\gamma}{2}\right\} \quad \text{and} \quad \Psi_\mathcal{C}^r = \left\{(\alpha, \beta) \;\middle|\; \beta = \frac{1+\gamma}{2}\right\},$$

which represent the two lines in parameter space, which separate the periodicity region $\mathcal{P}_\mathcal{C}$ from the rest of the discontinuous flat top tent map's dynamical behaviour.

It was shown in Sec. 2.1, that the periodicity region of each stable periodic orbit $\mathcal{O}_{\mathcal{C}\varrho}$ is given by a preimage of $I_\mathcal{C}$, and that at least for $\alpha > \alpha^\star$ this preimage is always complete, meaning that every point in $\overline{I_\mathcal{C}}$ has a preimage under f_ϱ^{-1}. Consequently, the BC curves of all these orbits can be derived from those of the fixed point:

$$\Psi^l_{\mathcal{C}\varrho} = \left\{ (\alpha,\beta) \;\middle|\; \beta = f_\varrho^{-1}\left(\tfrac{1-\gamma}{2}\right) \right\} \quad \text{and} \quad \Psi^r_{\mathcal{C}\varrho} = \left\{ (\alpha,\beta) \;\middle|\; \beta = f_\varrho^{-1}\left(\tfrac{1+\gamma}{2}\right) \right\}, \tag{3.7}$$

These curves in parameter space shall be denoted as the *endogenous border collision curves* of the orbit $\mathcal{O}_{\mathcal{C}\varrho}$, because they represent the case when the point $x_0 \in I_\mathcal{C}$ of this orbit collides with one of the borders of the middle partition from within. Note that the endogenous BC curves of every periodic orbit[3] intersect at either $(\alpha = +\infty, \beta = 0)$ or $(\alpha = +\infty, \beta = 1)$. Furthermore, the relative location of $\Psi^l_{\mathcal{C}\varrho}$ and $\Psi^r_{\mathcal{C}\varrho}$ in β-direction depends on the parity of ϱ, as for odd orbits the situation is mirrored with respect to the fixed point region $\mathcal{P}_\mathcal{C}$.

In contrast to the stable fixed point $\mathcal{O}_\mathcal{C}$ however, the periodicity regions $\mathcal{P}_{\mathcal{C}\varrho}$ are bounded not only by the two endogenous BC curves, but also by a third border collision bifurcation. For example, in Fig. 3.8 we can see that the periodicity region $\mathcal{P}_{\mathcal{CR}}$ (shown in a pale green) is "overshadowed" from below by the periodicity region of the fixed point. In this case, $\mathcal{P}_{\mathcal{CR}}$ is bounded by the three curves $\Psi^l_{\mathcal{CR}}$, $\Psi^r_{\mathcal{CR}}$ and $\Psi^r_\mathcal{C}$.

In fact, in Sec. 3.1 we have seen that every periodicity region $\mathcal{P}_{\mathcal{C}\varrho}$ is bounded on one side by the endogenous BC bifurcation of another orbit, as long as α is within the emerging domain of the unstable orbit which gives rise to $\mathcal{O}_{\mathcal{C}\varrho}$. This is the reason why the periodicity regions of an incrementing cascade lie densely adjacent to each other.

Fig. 3.8 shows an example of such an incrementing cascade around the curve $\mathcal{B}^\mathcal{R}_\mathcal{R}$, with the orbits $\mathcal{O}_{\mathcal{CR}^k}$, $k > 1$. As this is an odd incrementing cascade, each of the regions $\mathcal{P}_{\mathcal{CR}^k}$ borders on the region $\mathcal{P}_{\mathcal{CR}^{k-2}}$ on one side. This means that, for example, the periodicity region of the orbit $\mathcal{O}_{\mathcal{CR}^3}$ is bounded by its own endogenous BC curve $\Psi^r_{\mathcal{CR}^3}$ on one side, but by the curve $\Psi^r_{\mathcal{CR}}$ of its neighbour on the other. In this case, when traversing the latter bifurcation curve for increasing β, the symbolic dynamics of the discontinuous flat top tent map changes in the following way:

$$\mathcal{CR}\underline{\mathcal{R}}\mathcal{R} \to \mathcal{CR}$$

This means that the third point $x_2 \in \mathcal{R}$ (with the corresponding symbol underlined above) of the stable periodic orbit $\mathcal{O}_{\mathcal{CR}^3}$ collides from *outside* with the right boundary of the middle partition $I_\mathcal{C}$. This bifurcation is therefore referred to as the *exogenous border collision bifurcation* of this particular orbit, and the corresponding bifurcation curve is denoted by $\Phi_{\mathcal{CR}^3}$. In general, we can say that each[4] periodicity region $\mathcal{P}_{\mathcal{C}\varrho}$ is bounded by the three BC curves

$$\Psi^l_{\mathcal{C}\varrho}\,, \quad \Psi^r_{\mathcal{C}\varrho} \quad \text{and} \quad \Phi_{\mathcal{C}\varrho}.$$

[3] except for the fixed point $\mathcal{O}_\mathcal{C}$

[4] again, with the exception of the fixed point region $\mathcal{P}_\mathcal{C}$

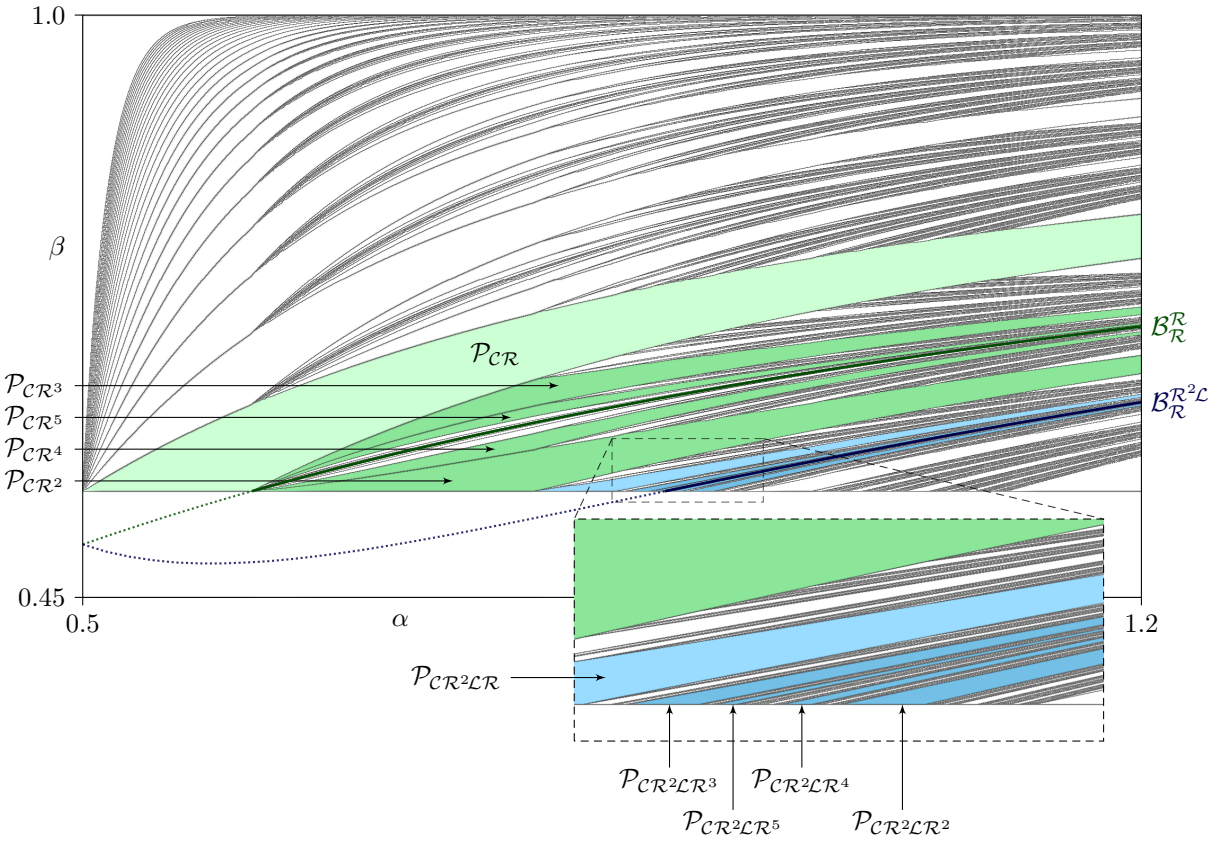

Figure 3.8: Two cases of incrementing cascades with the increment $\mathcal{R}$. The orbits $\mathcal{O}_{\mathcal{CR}^k}$, $k > 1$ originate from a single big bang bifurcation, and each exogenous BC curve $\Phi_{\mathcal{CR}^k}$ is given by $\Psi^{l/r}_{\mathcal{CR}^{k-2}}$. The orbits $\mathcal{O}_{\mathcal{CR}^2\mathcal{LR}^k}$ do not originate from a single bifurcation, but are spread out over α, and all exogenous BC curves $\Phi_{\mathcal{CR}^2\mathcal{LR}^k}$ are given by $\Psi^r_{\mathcal{C}}$.

Which point of the orbit exactly collides in the exogenous bifurcation at $\Phi_{\mathcal{C}\varrho}$ is determined by the respective incrementing cascade, in which the orbit $\mathcal{O}_{\mathcal{C}\varrho}$ is created.

Proposition 3.1. *If the orbit $\mathcal{O}_{\mathcal{C}\varrho}$ lies within the incrementing cascade corresponding to the Milnor attractor curve $\mathcal{B}^{\tilde{\varrho}}_{\sigma}$, which originates at the emerging point α_σ,[5] then the colliding point in the exogenous BC bifurcation $\Phi_{\mathcal{C}\varrho}$ is given by the first letter of the suffix σ for even cascades, or of the suffix σ^2 for odd cascades.*

This follows straightforward from Theorems 3.1 and 3.2. To take two examples from the cascades shown in Fig. 3.7: The exogenous BC bifurcation for the orbit $\mathcal{O}_{\mathcal{CLRL}(\mathcal{RRL})^2}$ in the even incrementing cascade corresponding to $\mathcal{B}^{\mathcal{LRL}}_{\mathcal{RRL}}$ is given by the collision of the orbit's 8th point with the right border of $I_{\mathcal{C}}$, or in symbolic notation

$$\mathcal{CLRLRRL}\underline{\mathcal{R}}\mathcal{RL}.$$

[5] This implies that the symbolic sequence of this orbit is of the form $\mathcal{C}\varrho = \mathcal{C}\tilde{\varrho}\sigma^k$.

The exogenous BC bifurcation for the orbit $\mathcal{O}_{\mathcal{CRRL}(\mathcal{LRL})^2}$ in the odd incrementing cascade corresponding to $\mathcal{B}^{\mathcal{RRL}}_{\mathcal{LRL}}$ is given by the collision of the orbit's 5^{th} point with the left border of $I_{\mathcal{C}}$, or in symbolic notation

$$\mathcal{CRRL}\underline{\mathcal{L}}\mathcal{RLLRL}.$$

Note that neither the existence of a family of orbits with sequences $\mathcal{C}\varrho\sigma^k$, nor the existence of any Milnor attractor curve $\mathcal{B}^{\varrho}_{\sigma}$ constitutes the necessary conditions for the aforementioned proposition. For example, consider the periodicity regions $\mathcal{P}_{\mathcal{CR}^2\mathcal{LR}^k}$, which are shown in Fig. 3.8 together with the Milnor attractor curve $\mathcal{B}^{\mathcal{R}^2\mathcal{L}}_{\mathcal{R}}$. For all these orbits, the exogenous bifurcations at $\Phi_{\mathcal{CR}^2\mathcal{LR}^k} = \Psi^r_{\mathcal{C}}$ are given by the collision of the respective orbit's second point $x_1 \in \mathcal{R}$ with the right boundary of $I_{\mathcal{C}}$.

All these orbits, although they can obviously be regarded as increments of $\mathcal{R}$, do not emerge at $\alpha_{\mathcal{R}}$ and therefore don't constitute a dense incrementing cascade as described by Theorems 3.1. Rather, the orbits $\mathcal{O}_{\mathcal{CR}^2\mathcal{LR}^k}$ appear successively along the α-axis, each emerging as part of a different incrementing cascade. The reason for this is that the Milnor attractor $\mathcal{B}^{\mathcal{R}^2\mathcal{L}}_{\mathcal{R}}$ appears as part of a homoclinic bifurcation of the unstable fixed point $\mathcal{O}_{\mathcal{R}}$, *after* the emerging point $\alpha_{\mathcal{R}}$.

In cases where the orbit lies at the brim of an incrementing cascade, the colliding point can be found by determining the adjacent periodicity region.

4 A System on Five Partitions

Consider the map given by

$$x_{n+1} = f\big(x_n\big) \quad \text{with} \quad f(x) = \begin{cases} \epsilon & F(x) < \epsilon \\ 1-\epsilon & F(x) > 1-\epsilon \\ F(x) & \text{otherwise} \end{cases} \tag{4.1}$$

where

$$F(x) = x\left(1 + \gamma(1-\varphi)(1-x)\left(\tfrac{1}{2x(1-\varphi)+2\varphi} + \tfrac{1}{2x(1-\varphi)-2}\right)\right). \tag{4.2}$$

This map, shown in Fig. 4.1, models an economic system which is introduced in [1] and describes an extension of the so-called Footloose Capital model. In this model, manufactured goods are produced and consumed in two separate regions. For some of these products, actors can choose to migrate factors of production between these two regions (therefore the term 'footloose') in order to increase profitability. Other products can only be manufactured in a certain region. The model includes a "trade freeness" parameter φ, which represents the reciprocal transport cost, and a gain parameter γ which models the speed with which each actor adjusts his production process in response to changes in the system. For a more detailed description, see [1].

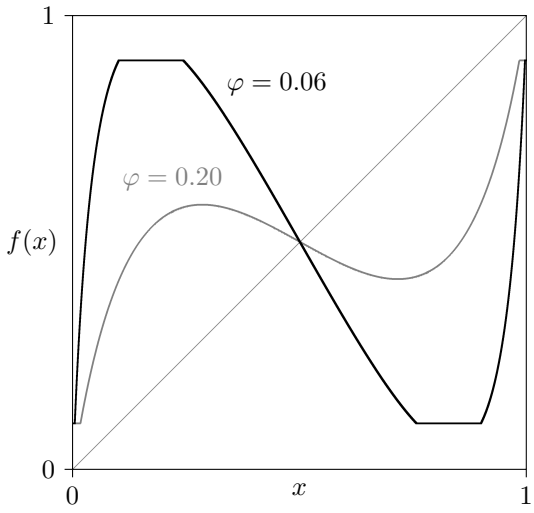

Figure 4.1: The extended Footloose Capital model given by (4.1) for $\gamma = 3.5$, $\varepsilon = 0.1$ and different values of φ.

It is worth noting that the function (4.2) has three fixed points $F(0) = 0$, $F\big(\frac{1}{2}\big) = \frac{1}{2}$ and $F(1) = 1$, and is symmetric to the point $\big(\frac{1}{2}, \frac{1}{2}\big)$, i.e.

$$F(x) = 1 - F(1 - x). \tag{4.3}$$

For $\varphi \neq 1$, $F(x)$ is continuous on $x \in [0, 1]$. In order to investigate the dynamical properties of this system from a new angle, we can now proceed exactly as with the flat top tent map in [2], by introducing the following *discontinuous* piecewise linear system, which is shown in Fig. 4.2:

$$g(x) = \begin{cases} g_L(x) = ax & \text{if} \quad 0 \leq x \leq \delta \\ g_{C_1}(x) = e & \text{if} \quad \delta < x < \frac{1}{2} - \delta \\ g_M(x) = \frac{1-2a\delta}{2\delta}\big(x - \frac{1}{2}\big) + \frac{1}{2} & \text{if} \quad \frac{1}{2} - \delta \leq x \leq \frac{1}{2} + \delta \\ g_{C_2}(x) = 1 - e & \text{if} \quad \frac{1}{2} + \delta < x < 1 - \delta \\ g_R(x) = a\big(x - 1\big) + 1 & \text{if} \quad 1 - \delta \leq x \leq 1 \end{cases} \tag{4.4}$$

Remark: for some orientation as to how a might be related to the original parameters (γ, φ), note that the slope of F in the origin is given by

$$\left.\frac{\mathrm{d}F(x)}{\mathrm{d}x}\right|_{x=0} = 1 + \frac{\gamma}{2\varphi}\big(1 - \varphi\big)^2.$$

Note that, similar to the parameter β of the discontinuous flat top tent map, e may be varied independently, and the continuous case is given by $e = a\delta$. In this case,

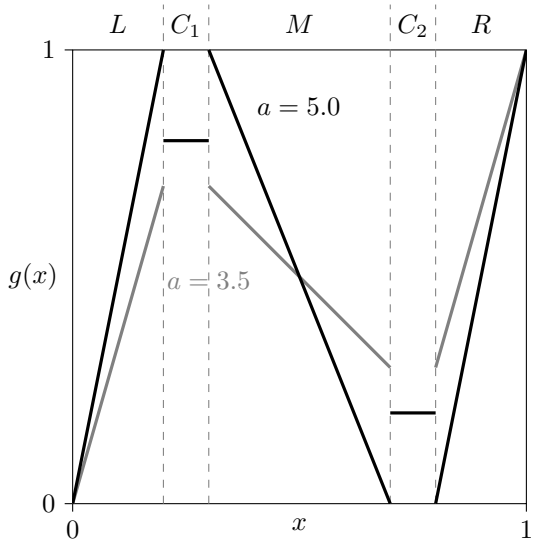

Figure 4.2: The discontinuous piecewise-linear system given by (4.4) for $\delta = 0.2$, $e = 0.8$ and different values of a.

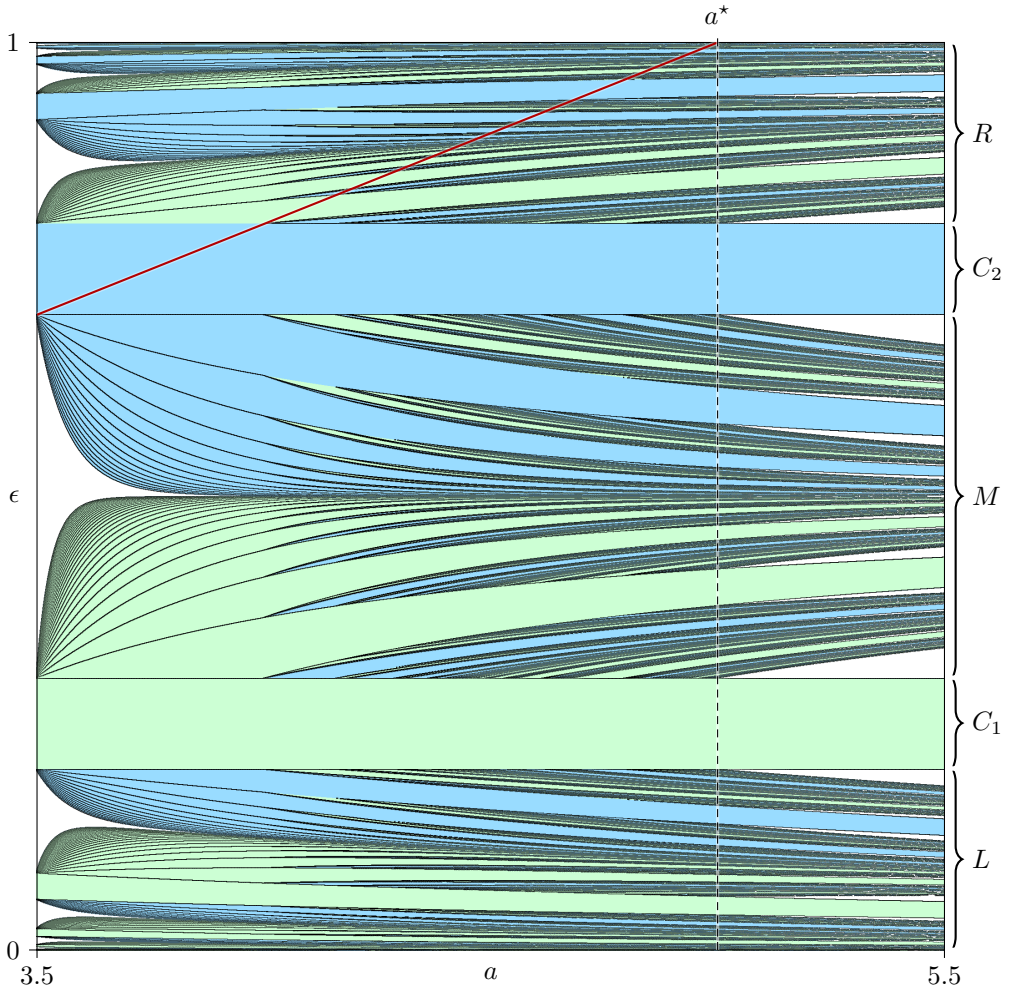

Figure 4.3: 2D bifurcation structure of (4.4) in the (a, e)-plane for $\delta = 0.2$, showing the curves separating regions of different period. The green regions correspond to preimages of I_{C_1} (these turn out to be periodicity regions with two coexisting orbits), whereas in the blue regions correspond to preimages of I_{C_2} (here, only one globally attracting cycle exists). The red line shows the case $e = a\delta$, where the system is continuous, as the original system (4.1).

(4.4) can be interpreted as an approximation of (4.1) (ignoring the original map's dynamically irrelevant[1] constant branches in the neighbourhoods of $x = 0$ and $x = 1$).

The bifurcation diagram of (4.4) for $\delta = 0.2$, $a \in [3.5, 5.5]$ and $e \in [0, 1]$ is depicted in Fig. 4.3 and shows strong structural similarities with the bifurcation diagram of the discontinuous flat top tent map (Fig. 2.2).

This simplified map is now defined on five partitions and possesses *two* constant function branches g_{C_1} and g_{C_2}, as opposed to the single constant branch $f_{\mathcal{C}}$ of the discontinuous flat top tent map. Note that, in the parameter region of Fig. 4.3,

[1] cf. the investigation of the system's parameter space in [1]

the function branches are increasing-constant-decreasing-constant-increasing, in that order. This corresponds to the shape of (4.1) for equivalently chosen parameters, as $F(x)$ is a bimodal function for $\gamma > \frac{(\varphi+1)^2}{(\varphi-1)^2}$.

For symbolic analysis, the partitions of this system shall be denoted as

$$I_L,\ I_{C_1},\ I_M,\ I_{C_2} \text{ and } I_R$$

from left to right, and the symbolic sequences defined accordingly. Analogous to the discontinuous flat top tent map, there is a special case where the map given by $g(x)$ is surjective, i.e. the non-constant branches g_L, g_M and g_R all map their respective domains onto $[0, 1]$. This holds for $a = a^\star = \frac{1}{\delta}$.

Here we can now argue exactly as in Sec. 2.2 with the successive subdivision of common-prefix regions, in order to generate a complete order of periodicity regions. First we must redefine the parity of a symbolic sequence $s \in \{L, C_1, M, C_2, R\}^n$ (or $\sigma \in \{L, M, R\}^n$ accordingly) following Definition 2.1. The parities of the symbols, according to the slopes of the corresponding branches of the map, are now of course

$$\text{par}(L) = 0,\ \text{par}(C_1) = 0,\ \text{par}(M) = 1,\ \text{par}(C_2) = 0 \text{ and } \text{par}(R) = 0.$$

Now the order of periodicity regions can be generated by

- ... subdividing the unit interval into $\{I_L,\ P_{C_1},\ I_M,\ P_{C_2},\ I_R\}$,
- ... subdividing each common-prefix region I_σ where σ is *even* into the regions $\{I_{\sigma L},\ P_{\sigma C_1},\ I_{\sigma M},\ P_{\sigma C_2},\ I_{\sigma R}\}$ and
- ... subdividing each common-prefix region I_σ where σ is *odd* into the regions $\{I_{\sigma R},\ P_{\sigma C_2},\ I_{\sigma M},\ P_{\sigma C_1},\ I_{\sigma L}\}$, i.e. in reverse order.

Corresponding to the example (2.7) of the discontinuous flat top tent map on p. 7, this is the second level of subdivision for the map (4.4):

$$\underbrace{\underbrace{I_{L^2} \mid P_{LC_1} \mid I_{LM} \mid P_{LC_2} \mid I_{LR}}_{I_L} \mid P_{C_1} \mid \underbrace{I_{MR} \mid P_{MC_2} \mid I_{M^2} \mid P_{MC_1} \mid I_{ML}}_{I_M} \mid P_{C_2} \mid \underbrace{I_{RL} \mid P_{RC_1} \mid I_{RM} \mid P_{RC_2} \mid I_{R^2}}_{I_R}}_{I=[0,1]}$$

4.1 Coexisting and Concatenated Orbits

There is now an important difference to the discontinuous flat top tent map in how this *order of periodicity regions* determines the *actual bifurcation structure*. The regions $P_{\sigma C_i}$ are not necessarily periodicity regions of only *one* periodic orbit, neither is the period of the existing orbit(s) directly equal to the length of the symbolic sequence which identifies the periodicity region. For example, all points $x \in P_{\sigma C_1}$, after a short trajectory with the symbolic sequence σ, are mapped to the partition I_{C_1}. How the

orbit continues after that is determined by the value of e. This can lie on either of the stable sets of I_{C_1} and I_{C_2}, i.e.

$$e \in \bigcup_{\sigma} P_{\sigma C_1} \quad \text{or} \quad e \in \bigcup_{\sigma} P_{\sigma C_2}, \quad \sigma \in \{L, M, R\}^n.$$

Due to the symmetry (4.3), the two constant function branches are related as follows:

$$e \in P_{s_0 s_1 \dots s_n} \iff (1-e) \in P_{\bar{s}_0 \bar{s}_1 \dots \bar{s}_n} \quad \text{where} \quad \bar{s}_i = \begin{cases} R & \text{if } s_i = L \\ C_2 & \text{if } s_i = C_1 \\ M & \text{if } s_i = M \\ C_1 & \text{if } s_i = C_2 \\ L & \text{if } s_i = R \end{cases}$$

Consequently, there are two possible cases for the dynamics of the system:

1. $e \in P_{\sigma C_1}$: two coexisting stable orbits with the sequence $C_1\sigma$ and $C_2\bar{\sigma}$

   $\implies P_{\sigma C_1} = \mathcal{P}_{\{C_1\sigma, C_2\bar{\sigma}\}}$

   (Regions of this kind are marked green in Fig. 4.3.)

2. $e \in P_{\sigma C_2}$: one globally attracting stable orbit with the sequence $C_1\sigma C_2\bar{\sigma}$

   $\implies P_{\sigma C_2} = \mathcal{P}_{C_1\sigma C_2\bar{\sigma}}$

   (Regions of this kind are marked blue in Fig. 4.3.)

In order to show that these results are also of relevance for the original map (4.1), the bifurcation diagram of this system is depicted in Fig. 4.4. When comparing this diagram to the one in Fig. 4.3, we can already see some structural similarities, such as the occurrence of coexisting and concatenated orbits. Of course, the respective parameter spaces for these two bifurcation diagrams have slightly different "semantics", as the system (4.1) is always continuous. To investigate the similarities further, we consider the case where (4.4) is also continuous. Therefore, $e = a\delta$ is chosen for the linearized map, which gives us the 1D bifurcation diagram shown in Fig. 4.5a. Furthermore, the original map shall be investigated in a region where its constant function branches (corresponding to I_{C_1} and I_{C_2} of (4.4)) are of constant width. For $\delta = 0.2$ the width of $I_{C_{1/2}}$ is 0.1, therefore the original system was investigated for 5 values of ϵ, and the following values of φ were determined numerically, for which the width of the constant branches of (4.1) is also 0.1:

ϵ	φ
0.000	0.0455488499
0.025	0.0500471927
0.050	0.0548659984
0.075	0.0600301923
0.100	0.0655679604

These points closely fit the linear relationship $\epsilon = 4.9895\varphi - 0.225481$, which is shown as a red line in the 2D bifurcation diagram in Fig. 4.4. With this restriction,

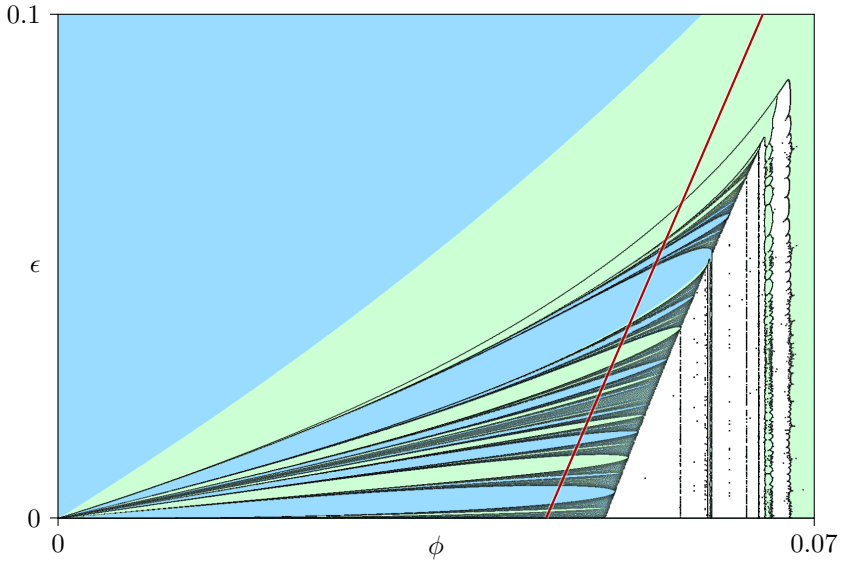

Figure 4.4: 2D bifurcation structure of (4.1) in the (ϕ, ϵ)-plane for $\gamma = 3.5$, showing the curves separating regions of different period. The green regions correspond to coexisting orbits, whereas in the blue regions correspond to orbits involving both flat branches. The red line shows the case in which the system's flat branches have an approximately constant width of 0.1, therefore corresponding to the continuous case of (4.4).

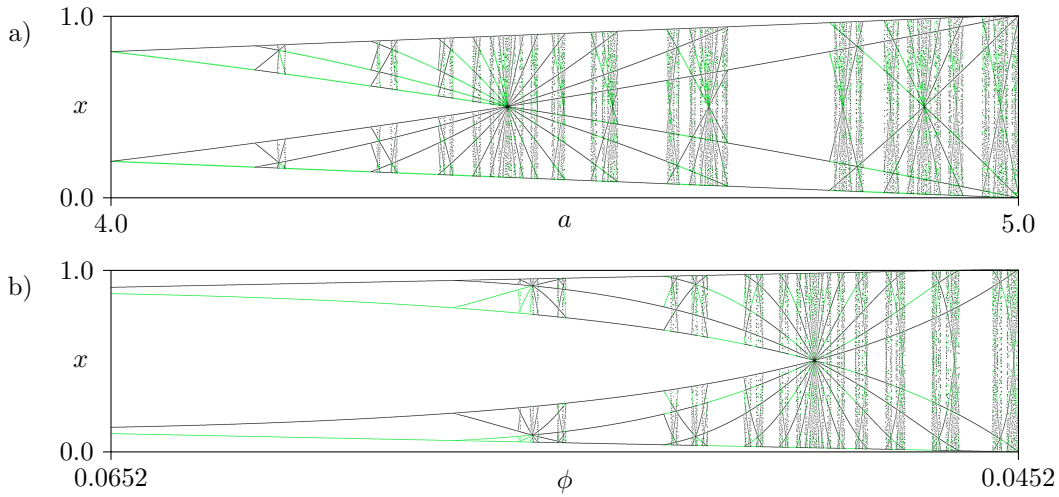

Figure 4.5: Comparison of the 1D bifurcation diagrams of the piecewise-linear map g and the extended Footloose Capital model f. a) diagram for (4.4) with $\delta = 0.2$ and the continuity condition $e = a\delta$. b) diagram for (4.1) with $\gamma = 3.5$ and the condition $\epsilon = 4.9895\varphi - 0.225481$, which approximates a constant flat branch width of 0.1. Coexisting orbits are shown in green.

we get the 1D bifurcation diagram shown in Fig. 4.5b. Comparing these two diagrams, we can see that, although the two systems obviously scale differently in their respective parameters, the bifurcation scenarios are in fact very similar.

4.2 Generalised Results

The results from above may also be generalised to a procedure for arbitrary n-partition systems of the same class, i.e. discontinuous piecewise-affine maps from an interval I onto itself with least one constant function branch.

Assuming the system's symbolic description is given as

- $A_1, A_2, \dots$ for all partitions with a *positive* slope,
- $B_1, B_2, \dots$ for all partitions with a *negative* slope and
- $C_1, C_2, \dots$ for all partitions where the system function is constant,

then the structure of the partitions can be represented as a list

$$\Big(I_{S_1}, I_{S_2}, \dots, I_{S_n}\Big), \quad I = \bigcup_{k=1}^{n} I_{S_k}, \quad S_i \in \big\{A_1, A_2, \dots, B_1, B_2, \dots, C_1, C_2, \dots\big\}.$$

In this notation the discontinuous flat top tent map, for example, would be given by $\big(I_{S_1}, I_{S_2}, I_{S_3}\big) = \big(I_{A_1}, I_{C_1}, I_{B_1}\big)$, and the extended Footloose Capital model (4.1) by $\big(I_{S_1}, I_{S_2}, I_{S_3}, I_{S_4}, I_{S_5}\big) = \big(I_{A_1}, I_{C_1}, I_{B_1}, I_{C_2}, I_{A_2}\big)$. The parity for the symbolic sequences $s \in \{S_k\}^n$ of all these systems can be defined uniformly as

$$\operatorname{par} s = \left(\sum_{i=1}^{n} \operatorname{par}\big(s_i\big)\right) \bmod 2, \quad \text{where} \quad \forall i \ \operatorname{par}\big(A_i\big) = \operatorname{par}\big(C_i\big) = 0, \ \operatorname{par}\big(B_i\big) = 1.$$

Now a "recipe" for generating the basic order of the preimages of the constant branches C_i can be stated as follows:

1. The map's domain I is subdivided into the partitions $\big(U_1, U_2, \dots, U_n\big)$

$$U_i = \begin{cases} I_{S_i} & \text{if } S_i \in \{A_k, B_k\} \\ P_{S_i} & \text{if } S_i \in \{C_k\}. \end{cases}$$

2. Each interval I_σ is further subdivided into partitions $\big(U_{k(1)}, U_{k(2)}, \dots, U_{k(n)}\big)$, where

$$k(i) = \begin{cases} i & \text{if } \operatorname{par}\sigma = 0 \\ n+1-i & \text{if } \operatorname{par}\sigma = 1 \end{cases} \quad \text{and} \quad U_i = \begin{cases} I_{\sigma S_i} & \text{if } S_i \in \{A_k, B_k\} \\ P_{\sigma S_i} & \text{if } S_i \in \{C_k\}. \end{cases}$$

3. Step 2 is repeated recursively.

The situation of coexisting and/or concatenated orbits can become more or less arbitrarily complex if all constant branches can be varied independently, but can easily be captured in a transition graph. For example, if our system has four constant branches $C_1 \dots C_4$ plus a number of branches with positive/negative slope, and we denote the values of the constant branches as β_i, one possible situation could be

$$\beta_1 \in P_{\sigma^I C_2}, \quad \beta_2 \in P_{\sigma^{II} C_3}, \quad \beta_3 \in P_{\sigma^{III} C_2} \quad \text{and} \quad \beta_4 \in P_{\sigma^{IV} C_4},$$

with the corresponding transition graph:

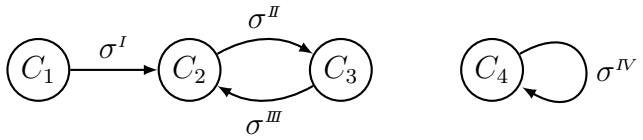

In this case, the system would possess two coexisting stable orbits, one with the sequence $C_2\sigma^{II}C_3\sigma^{III}$ (to which also the partition I_{C_1} is mapped), and the other with the sequence $C_4\sigma^{IV}$.

In conclusion, this procedure can help in determining the principal periodicity structure for a vast class of dynamical systems. As with the two maps that have been investigated in this thesis, one would need an additional existence condition in order to determine the concrete bifurcation scenarios occurring in such a system, for all typical parameter settings which lead the map under consideration to be non-surjective.

5 Conclusions

This work has shown that the nested period incrementing scenario can not only be concisely described on a global scale, as with the binary tree structure that was shown in Sec. 2, but also locally by regarding the structure of big bang bifurcations. These organising centers are accompanied by the appearance of unstable orbits and Milnor attractors in the system. Depending on the parity of these unstable orbits, two types of incrementing cascades can be generated at the corresponding big bang points. In the case with even parity, any existing periodicity region is augmented by two neighbouring cascades, where the periods increase monotonically in both directions. In the case with odd parity, each existing region is augmented by an alternating incrementing cascade. The investigation demonstrated that the resulting orbits can be easily classified using symbolic dynamics.

The α-order of these big bang bifurcations is partly determined by the U-sequence introduced by Metropolis, Stein and Stein. In this sense, the complete 2D structure of the nested period incrementing scenario can be produced by first applying their rules for the symbolic dynamics of the period doubling cascade, and extending the results using the rules developed in this work.

It has been shown that the techniques used and developed in this work can be used conveniently to investigate many-partition discontinuous systems with constant function branches.

Acknowledgements

Many thanks to my supervisors Viktor Avrutin and Michael Schanz for their help and suggestions, to Laura Gardini for pointing us to the Footloose Capital model, and to Marina for constant and loving support.

Bibliography

[1] A. Agliari, P. Commendatore, I. Foroni, and I. Kubin. Border Collision Bifurcations in a Footloose Capital Model with First Nature Firms. Manuscript submitted for publication, 2011.

[2] B. W. Futter. Investigation of a Discontinuous Piecewise Linear Map Defined on Three Partitions. Student thesis, University of Stuttgart, 2010.

[3] P. Jain and S. Banerjee. Border-Collision Bifurcations in One-Dimensional Discontinuous Maps. *International Journal of Bifurcation and Chaos*, 13(11):3341–3351, 2003.

[4] N. Metropolis, M. L. Stein, and P. R. Stein. On Finite Limit Sets for Transformations on the Unit Interval. *Journal of Combinatorial Theory, Series A*, 15(1):25–44, 1973.

[5] H. E. Nusse, E. Ott, and J. A. Yorke. Border-collision bifurcations: An explanation for observed bifurcation phenomena. *Physical Review E*, 49(2):1073–1076, 1994.

[6] I. Sushko and L. Gardini. Degenerate Bifurcations and Border Collisions in Piecewise Smooth 1D and 2D Maps. *International Journal of Bifurcation and Chaos*, 20(7):2045–2070, 2010.

Declaration

All the work contained within this thesis, except where otherwise acknowledged, was solely the effort of the author. At no stage was any collaboration entered into with any other party.

(Ben W. Futter)